Natural product antibiotics: synthesis and next generation analogues

Lysenko, V.

Chapter 5

Design, Synthesis, and Antibacterial Evaluation of Rifampicin-Siderophore Conjugates

Abstract

The growing concern over antibiotic resistance has sparked increased attention toward developing new antibiotic strategies. One promising approach, known as the "Trojan horse" strategy, involves the use of siderophores to hijack bacteria's iron transport systems as a way of delivering antibiotics inside the bacterial cell. This method is particularly promising in tackling Gram-negative bacteria, which have an outer membrane that many antibiotics cannot penetrate. One such antibiotic is rifampicin, a drug used to treat tuberculosis and infections caused by Gram-positive bacteria. Although rifampicin binds to a highly conserved bacterial RNA subunit, its activity is generally poor against Gram-negative bacteria due to their outer membrane. Aiming to expand rifampicin's efficacy, we here report the design and synthesis of several rifampicin-siderophore conjugates that exhibit enhanced activity against Gram-negative pathogens. Our findings indicate that the structural features of both the linker and catechol are crucial for the activity of conjugates with compound **33**, wherein rifampicin is connected to chlorocatechol via a short ester linker, showing an up to 32-fold improvement in activity.

Parts of this chapter have been published in:

Lysenko, V.*; Gao, M.-L.*; Sterk, F. A. C.; Innocenti, P.; Slingerland, C. J.; Martin, N. I. Design, Synthesis, and Antibacterial Evaluation of Rifampicin–Siderophore Conjugates. *ACS Infect. Dis.* **2025**, *11* (8), 2301–2309.

* - these authors contributed equally.

Introduction

The rapid emergence and global spread of multidrug-resistant (MDR) bacteria represent a significant public health crisis and pose substantial challenges to modern medicine.[1-3] Of particular concern are MDR Gram-negative pathogens, including *Escherichia coli*, *Klebsiella pneumoniae*, *Acinetobacter baumannii,* and *Pseudomonas aeruginosa*, which are associated with severe and often life-threatening infections such as sepsis, pneumonia, and urinary tract infections.[4] Due to their impermeable outer membrane (OM) and efficient efflux pumps, Gram-negative bacteria have generally proven to be more challenging to treat with antibiotics than Gram-positive pathogens.[5-7] The growing threat posed by infections due to MDR Gram-negative bacteria underscores the need for novel antibiotics that can overcome both their intrinsic and acquired resistance mechanisms.

In this study, we describe approaches to expanding the therapeutic utility of rifampicin by making it more active towards Gram-negative bacteria. Rifampicin (**Figure 1A**) is a potent inhibitor of bacterial RNA polymerase and is a cornerstone antibiotic for treating *Mycobacterium tuberculosis* infections and other diseases caused by Gram-positive bacteria.[8-11] While rifampicin exhibits similar inhibitory activity against RNA polymerase from both Gram-positive and Gram-negative bacteria, its clinical efficacy against Gram-negative bacteria is severely limited due to poor outer membrane permeability.[12,13] Despite these limitations, rifampicin's well-characterized mechanism of action makes it an attractive candidate for modifications aimed at overcoming its lack of OM permeability against Gram-negative pathogens. Furthermore, recent studies have shown that when used together with agents capable of inducing OM disruption, the antimicrobial activity of rifampicin is improved, likely due to increased access to its intracellular target.[14,15]

To enable rifampicin to breach the OM of Gram-negative bacteria as a means of enhancing its antibiotic efficacy, we opted to explore the so-called "Trojan horse" strategy. This approach involves exploiting the bacterial iron acquisition pathway, which is critical for bacterial growth and pathogenicity.[16-18] To acquire iron from environments where this critical resource is scarce, such as in mammalian hosts, bacteria synthesize and secrete siderophores that tightly bind exogenous iron and facilitate its uptake through specific outer membrane transporters.[19-21] Enterobactin (**Figure 1A**) is the preeminent naturally produced siderophore. Enterobactin's highly efficient iron binding is driven by the specific shape of its macrocycle and the positioning of the catechol rings, which induce the formation of a stable ferric complex.[22,23] The underlying idea of the "Trojan horse" strategy is to covalently link a siderophore-like moiety with an antibiotic that has poor OM permeability. This then allows for hijacking of the bacterial iron uptake system to transport the siderophore-antibiotic conjugate across the OM with subsequent release inside the cell.[17,24,25] Previous studies have shown that some rifamycin-siderophore conjugates bearing cleavable linkers can be transported inside bacteria, after which the rifamycin payload is released.[26] Also of note, analogues of rifampicin, such as rifabutin,

were also found to overcome the membrane permeability issue by hijacking an iron transporter to get inside the bacteria.[27-30] These findings suggest that rifampicin and its analogues may be particularly well suited to Trojan horse strategies as a means of enhancing their activity against Gram-negative bacteria.

A prime example of an antibiotic that exploits the "Trojan horse" approach is the FDA-approved drug – cefiderocol, which consists of a β-lactam core conjugated to a chlorocatechol moiety (**Figure 1A**). The chlorocatechol group significantly enhances the activity of cefiderocol compared to other β-lactam antibiotics and positions it as one of the few options for treating multidrug-resistant Gram-negative pathogens.[31-33] Building from this concept, we envisioned conjugating rifampicin to a similar chlorocatechol unit (**Figure 1B**) as a means of enhancing antibacterial activity against Gram-negative bacteria. Previous reports have identified the piperazine ring of rifampicin as an exploitable site for chemical modification, given that it is not directly involved in binding to the RNA polymerase active site.[34,35] This is an important consideration given the need to ensure that the conjugate preserves rifampicin's inhibitory function while permitting structural modifications that facilitate siderophore-mediated uptake. Here, we report the synthesis and evaluation of a series of rifampicin-siderophore conjugates incorporating linkers with different properties and lengths. By optimizing the linker, we successfully identified a subset of conjugates with enhanced antibacterial activity and assessed the contribution of the bacterial iron uptake system to this activity.

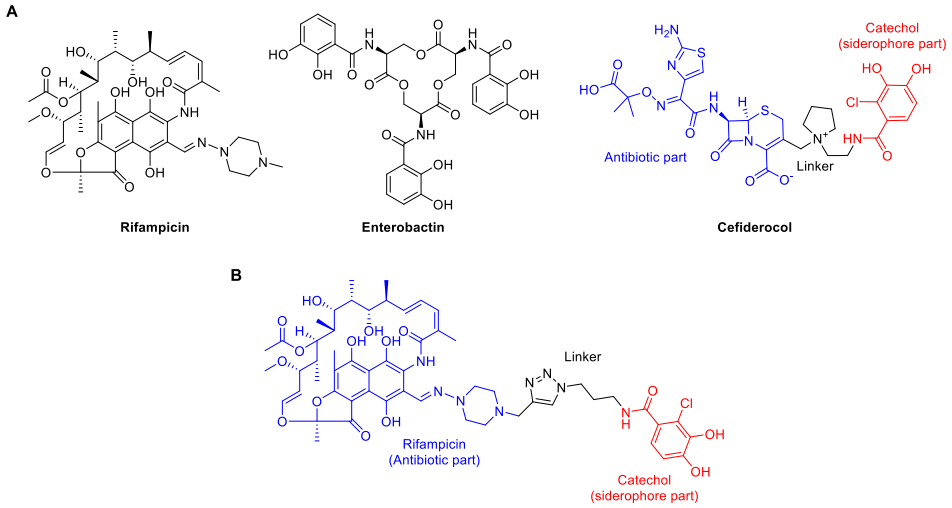

Figure 1. **A)** Structures of rifampicin, enterobactin and cefiderocol. **B)** Prototype rifampicin-siderophore conjugate (**1**).

Results and discussion

In designing a prototype conjugate of rifampicin and the chlorocatechol unit derived from cefiderocol, we elected to first apply an azide-alkyne "click-chemistry" ligation strategy to provide convenient access to conjugate **1** via well-described methods.[36-39] The key building blocks needed for our strategy were the previously reported rifampicin alkyne **2**,[39,40] and catechol-azide **7** (**Scheme 1**). In doing so, azido amine **4** was first generated by azide displacement of the corresponding 3-chloro propylamine. Carboxylic acid **6** was then prepared via the BBr_3-mediated demethylation of commercially available **5** and coupled to **4** to yield catechol-azide **7**. Conventional click-chemistry conditions were then used to ligate alkyne **2** (made as illustrated in **Scheme S1**) and azide **7**, yielding conjugate **1**. In addition to conjugate **1**, compounds **8-12** were also prepared as a series of controls to allow for the assessment of the contributions of the triazole and chlorocatechol moieties (**Scheme S2**) relative to unmodified rifampicin.

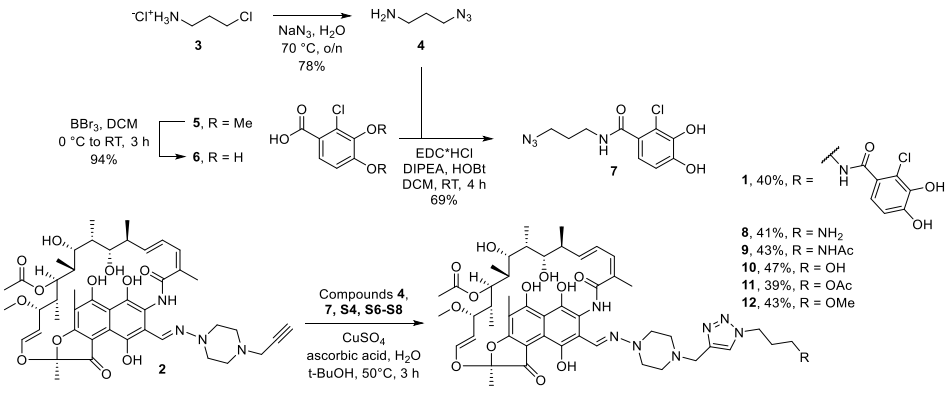

Scheme 1. Synthesis of the conjugates using the click-chemistry approach.

The activity of conjugate **1** was then assessed against a panel of Gram-negative bacteria (**Table 1**). Minimum inhibitory concentration (MIC) values were determined using standard broth dilution assays and compared to those measured for authentic rifampicin. Given that the impact of siderophore-mediated transport is most effective at low iron concentrations,[41] the MIC assays were run using iron-depleted, cation-adjusted Mueller-Hinton broth (ID-CAMHB) as the growth medium. Rather unexpectedly, the results of these MIC assays showed that the antibacterial activity of conjugate **1** was consistently lower than that of unmodified rifampicin. Activity was reduced 8-fold against *E. coli* ATCC 25922 and 16-fold against *A. baumannii* ATCC 19606. Furthermore, **1** showed no measurable activity against *K. pneumoniae* ATCC 13883 and *P. aeruginosa* ATCC 10145. Only against *E. coli* BW 25113 was the activity of compound **1** equivalent to that of rifampicin.

Table 1. MICs of compounds **1**, **33-39**, and rifampicin in CAMHB (iron-rich medium) and ID-CAMHB (iron-poor medium) against a panel of Gram-negative bacteria.

Strain	MIC (μg/mL)								
	1*	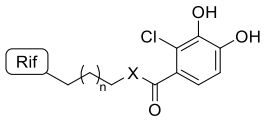				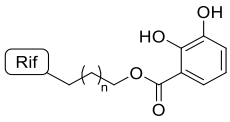			Rif
		33 n = 1 X = O	**34** n = 3 X = O	**35** n = 5 X = O	**39** n = 1 X = NH	**36** n = 1	**37** n = 3	**38** n = 5	
Iron-rich medium									
E. coli BW 25113	>64	2	4	64	8	16	>64	>64	8
E. coli JW 3594 *ΔrfaD*	4	1	2	8	4	4	4	4	0.25
E. coli BW 25113 *ΔbamB ΔtolC*	2	1	2	8	2	4	4	32	1
Iron-poor medium									
E. coli BW 25113	32	1	2	4	2	8	64	64	8
E. coli ATCC 25922	8	2	4	8	16	8	32	>64	8
A. baumannii ATCC 19606	32	0.5	1	2	4	4	4	>64	2
K. Pneumoniae ATCC 13883	>64	2	2	>64	8	64	>64	>64	32
P. aeruginosa ATCC 10145	>64	1	>64	>64	32	>64	>64	>64	16

*For the structure of conjugate **1** see **Figure 1**.

Given these findings, we proceeded to test compound **1** against two well-characterized OM-disrupted *E. coli* mutants: *E. coli* JW 3594 *ΔrfaD* (with the gene responsible for LPS biosynthesis knocked out) and *E. coli* BW 25113 *ΔbamB ΔtolC* (with deletions of the BamB gene alongside knockout of the TolC porin gene).[42,43] These assays were conducted to assess whether **1** shows activity against hypersensitive strains in which the OM is compromised. We also included compound **2** to assess whether the alkyne substituent has any effect on rifampicin's activity (**Table 2**). As expected, we found that rifampicin exhibits activity against the membrane-disrupted strains. Conversely, we observed that conjugate **1** again displayed reduced activity against both strains, with the largest reduction (8-fold) against the *ΔrfaD* strain. In comparison, compound **2** was found to have similar MIC values to rifampicin, with no significant reduction in activity. These findings suggested that the triazole-based linker strategy used in conjugate **1** may result in reduced binding to the target RNA polymerase. To investigate whether the introduction of the triazole was the key factor in the conjugate's diminished antimicrobial potency, we

therefore prepared and tested a series of triazole-modified rifampicin analogues terminating in amine, alcohol, amide, ester, or ether moieties (compounds **8-12**, **Scheme 1**) to estimate a possibility of modifying rifampicin via a click-chemistry conjugation approach without affecting its activity. These compounds were tested against wild-type *E. coli* BW 25113, membrane-disrupted *E. coli* JW 3594 *ΔrfaD*, and *E. coli* BW 25113 *ΔbamB ΔtolC*. In all cases, the activities of the triazole-bearing compounds were reduced relative to rifampicin (**Table 2**), further indicating that triazole-based linkers, which include the use of building block **2**, negatively impact antibacterial potency.

Table 2. MICs of compounds **2**, **8-12**, **21-23** compared to rifampicin against wild-type *E. coli* and membrane-deficient *ΔrfaD* and *ΔbamB ΔtolC* strains in CAMHB (iron-rich medium).

Strain	MIC (μg/mL)									
	2*	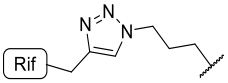					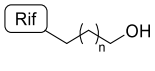			Rif
		8 NH_2	**9** NHAc	**10** OH	**11** OAc	**12** OMe	**21** n = 1	**22** n = 3	**23** n = 5	
E. coli BW 25113	16	>64	>64	>64	64	32	8	16	16	8
E. coli JW 3594 *ΔrfaD*	0.25	8	>8	1	2	0.5	0.5	0.5	0.5	0.25
E. coli BW 25113 *ΔbamB ΔtolC*	2	2	4	4	4	4	2	2	2	1

*For the structure of compound 2 see **Scheme 1**.

In light of these findings, we proceeded to explore alternative linking strategies not dependent on alkyne-azide ligation. To this end, we designed a series of ester-linked conjugates wherein the rifampicin piperazine was substituted with an alkyl linker, terminating with an alcohol group to which the catechol carboxylic acid would be coupled. To accommodate variations in the linker, we designed a synthetic route that would allow for the most divergent approach (**Scheme 2**). Starting from Boc-protected piperazine **13**, reaction with *tert*-butyl nitrite yielded *N*-nitroso compound **14** quantitatively. Reduction using zinc with NH_4Cl afforded hydrazine **15**, which was subsequently protected with a Cbz group, resulting in piperazine **16**. Treatment with TFA in DCM, followed by evaporation and trituration, afforded compound **17** as a TFA salt in multigram quantities. Protected piperazine **17** was then alkylated with three different bromo alcohols of varying lengths to give building blocks **18-20** in good yields. Following the removal of the Cbz group by hydrogenation, the piperazines were condensed with the commercially available rifaldehyde to yield compounds **21-23**. Before coupling **21-23** with the catechol carboxylic acid, we tested their activities against a panel of bacteria to assess the impact of the linkers. The results of these assays were encouraging, with substituted rifampicin building blocks **21-23** showing activity similar

to that of the parent antibiotic (**Table 2**). Encouraged by these findings, we proceeded to generate the corresponding rifampicin-siderophore conjugates connected by an ester linkage.

Two different catechol fragments were chosen as building blocks for the ester-linked rifampicin conjugates: the chlorocatechol featured in compound **1** (derived from the structure of cefiderocol) and a simpler nonchlorinated variant inspired by the catechol unit of enterobactin. In doing so, we generated a set of six rifampicin-siderophore conjugates consisting of alkyl linkers of three different lengths and two different catechol moieties (**Scheme 3**). The protected catechol building blocks required for our synthetic strategy were prepared from compounds **6** and **24** via reaction with benzyl bromide in acetone, followed by aqueous basic hydrolysis to obtain the benzoic acid derivatives **25** and **26**. Using DIC/DMAP activation, **25** and **26** were then coupled to the previously obtained Cbz-protected aminopiperazine-based alcohols **18**-**20** to give the protected ester intermediates. Following the work-up, the protected ester products were directly treated with Pd/C under a hydrogen atmosphere to simultaneously remove the Cbz and benzyl groups. This gave building blocks **27**-**32**, which were then condensed with rifaldehyde to yield rifampicin-siderophore conjugates **33**-**38**. The antibacterial activities of **33**-**38** were then evaluated against the same panel of strains previously used for compound **1** and again in iron-poor medium (**Table 1**).

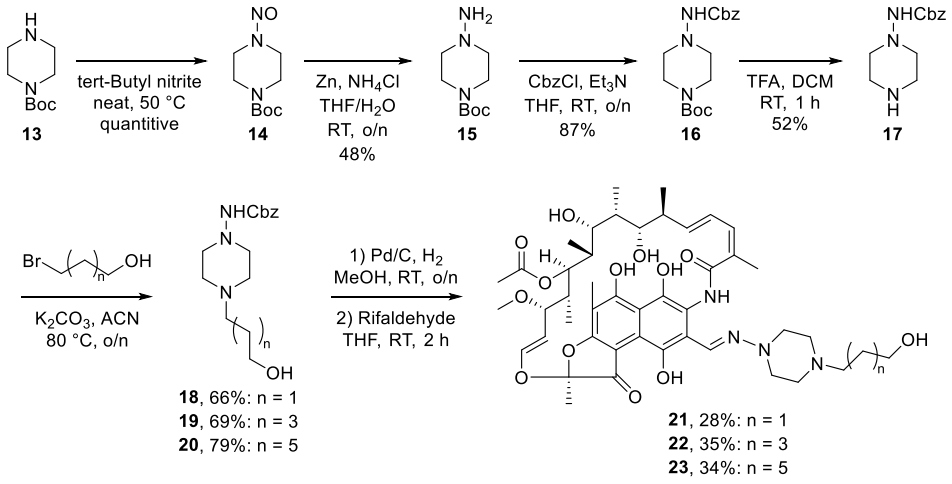

Scheme 2. Synthesis of the rifampicins modified with different alcohol-containing linkers.

We were pleased to find that some of the ester-linked conjugates demonstrated an antimicrobial profile equivalent to or better than that of rifampicin itself, with compound **33**, bearing the three-carbon linker and chlorocatechol moiety, being the most potent overall. Conjugates **33**-**38** were also found to be non-hemolytic, indicating that the enhanced antibacterial activities observed are not due to nonspecific membrane disruption (**Figure S1**). Additionally, in MIC assays using membrane-deficient strains, **33** showed

activity comparable to that of rifampicin (**Table 1**). This finding suggests that the ester linkage does not interfere with target binding as much as the triazole-based linker used in the initial design of conjugate **1**. The most considerable increase in potency observed for compound **33** relative to rifampicin (16-fold) was found against strains of *K. pneumoniae* and *P. aeruginosa*, whose proliferation was interestingly not at all affected by treatment with compound **1** (**Table 1**). Upon comparing the activity of the rifampicin-siderophore conjugates, we noticed a number of interesting correlations. First, conjugates derived from chlorocatechol **6** appeared more potent than those derived from catechol **24**. For example, when comparing compound **36** to compound **33**, which differ only in the substitution pattern on the bisphenol ring, we noticed a 4- to 64-fold difference in the MICs, suggesting that the chloro-containing catechol derived from cefiderocol has a beneficial effect on the activity compared to the simpler catechol derived from enterobactin. A similar trend, favoring the activity of chloro-substituted conjugates, was observed for other compounds with longer linkers. Additionally, we found that the distance between the rifampicin core and the catechol portion has an impact on the antimicrobial potency. The data summarized in **Table 1** show that analogue **33** is more potent than **34**, which in turn is more active than **35**. This trend, also shared by conjugates **36**-**38**, incorporating the catechol derived from enterobactin, suggests a preference for the shorter linker.

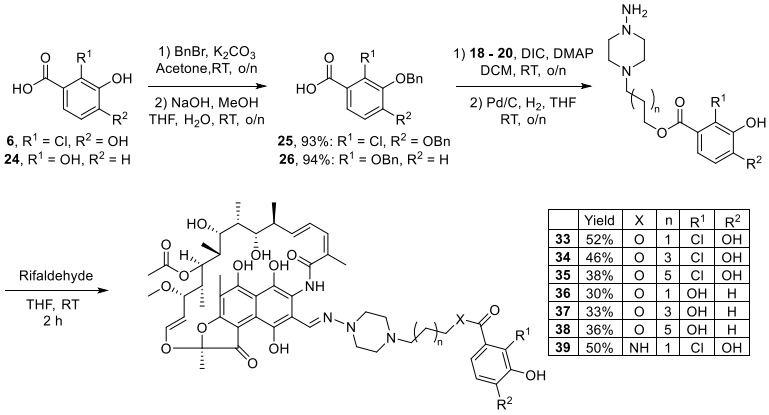

	Yield	n	R^1	R^2
27	46%	1	Cl	OH
28	50%	3	Cl	OH
29	40%	5	Cl	OH
30	14%	1	OH	H
31	58%	3	OH	H
32	41%	5	OH	H

	Yield	X	n	R^1	R^2
33	52%	O	1	Cl	OH
34	46%	O	3	Cl	OH
35	38%	O	5	Cl	OH
36	30%	O	1	OH	H
37	33%	O	3	OH	H
38	36%	O	5	OH	H
39	50%	NH	1	Cl	OH

Scheme 3. Synthesis of the rifampicin-siderophore conjugates.

Given that conjugate **33** contains an ester linkage between rifampicin and the chlorocatechol moiety, we elected to also synthesize the corresponding amide analogue **39** to assess whether the more stable and synthetically convenient amide-linked variant is also more active than rifampicin. The synthesis of **39** was carried out following the same route depicted in **Scheme 3**, but employing the amide-linked intermediate **S12** in the final condensation with rifaldehyde (**S12** was prepared in five steps from Cbz-protected *N*-aminopyperazine **17**, as illustrated in **Scheme S3**). Interestingly, when tested against the same panel of Gram-negative bacteria, conjugate **39** was found to have consistently reduced antibacterial activity relative to both ester-linked **33** and rifampicin. This finding

may provide insights into the working mechanism of these conjugates. In the case of **33**, siderophore-mediated entry into the bacterial cell might be followed by the hydrolysis of the ester linkage to release active compound **21** (**Table 2**). In contrast, the same pathway is less likely with **39**, due to the greater hydrolytic stability of the amide linkage. However, based on the data presented, it cannot be conclusively stated that the decreased potency observed for **39** is due to linker stability. Other possible effects, such as reduced uptake of **39** by outer membrane transporters or decreased binding to the target RNA polymerase, could also explain the reduced activity observed.

Given the strongly enhanced activity of conjugate **33** relative to rifampicin when tested against strains used in the preliminary screen, the compound was further evaluated against a broader panel of clinical isolates with different resistance mechanisms (**Table 3**). Again, **33** displayed enhanced activity against almost all strains compared to rifampicin. While testing against a panel of different *E. coli* strains, the activity enhancement over rifampicin was from 4- to 32-fold, with the biggest increase of activity against the *E. coli* 2018-022 (VIM-2) strain. Meanwhile, good activity, with MICs ranging from 0.5 to 2 μg/mL, was also observed for a number of *A. baumannii* strains, including multidrug-resistant isolates, which are among the most clinically challenging classes of Gram-negative pathogens.[44,45] These MIC values correspond to a 2- to 8-fold improved activity over rifampicin, depending on the strain. Compound **33** also demonstrated enhanced potency against multiple-resistant *K. pneumoniae* strains, resulting in 4- to 16-fold lower MIC values compared to those measured for rifampicin. On the other hand, a number of the *P. aeruginosa* strains tested were not found to be more sensitive to conjugate **33**, showing similar MIC values as those of rifampicin, with the exception of *P. aeruginosa* NRZ-03961, where we observed a 16-fold increase in potency, similar to our findings with *P. aeruginosa* ATCC 10145 in the initial screen. The activity of conjugate **33** was also improved relative to rifampicin against highly colistin-resistant strains of *E. coli* pRIVM_C029515_2 and *K. pneumoniae* RIVM_C019741 acquired from hospitals in the Netherlands.[46] Interestingly, the *E. coli* RC0089 and *K. pneumoniae* NCTC 13443 strains, both bearing NDM-1 resistance, were found to be resistant to both rifampicin and conjugate **33**. This is possibly related to the finding that plasmids that harbor the NDM-1 gene are often associated with other resistance markers, including those conferring rifampicin resistance.[47]

Table 3. MICs of conjugate **33** and rifampicin in ID-CAMHB (iron-poor medium) against multiple bacterial strains, including drug-resistant clinical isolates.

Strain	MIC (μg/mL)	
	33	Rifampicin
E. coli BW 25113	1	8
E. coli ATCC 25922	2	8
E. coli NTCT 13846 (MDR)	2	16
E. coli MVAST0072 (MDR)	4	16
E. coli EQAS 2016 (mcr-1)	4	16
E. coli pRIVM_C029515_2 (mcr-1)	4	16
E. coli 2018-022 (VIM-2)	1	32
E. coli RC0089 (NDM-1)	>32	>64
A. baumannii ATCC 19606	0.5	2
A. baumannii ATCC 17978	1	8
A. baumannii NRZ-00687 (NDM-2)	1	4
A. baumannii RUH-134 (MDR)	2	8
A. baumannii 2018-006 (NDM/OXA-023/OXA-051)	2	4
A. baumannii KML-11668 (MDR)	1	2
K. pneumoniae ATCC 13883	2	32
K. pneumoniae NR-48977 (MDR)	4	64
K. pneumoniae NR-48978 (MDR)	4	64
K. pneumoniae RIVM_C019741 (colistin-resistant)	8	64
K. pneumoniae 1124 (VIM-1)	8	32
K. pneumoniae NCTC 13443 (NDM-1)	>32	>64
P. aeruginosa ATCC 10145	1	16
P. aeruginosa ATCC 27853	8	16
P. aeruginosa PAO1	16	16
P. aeruginosa NRZ-08418 (NDM-1)	16	16
P. aeruginosa 1427 (VIM-2)	8	8
P. aeruginosa NRZ-03961 (IMP-1)	0.5	8

The role of available iron and iron transport on the activity of the rifampicin-siderophore conjugates was further investigated. In doing so, we directly compared the antibacterial activities of **33-39** in iron-rich and iron-depleted media (**Table 1**). In all cases, the MIC values measured for our conjugates were heightened when tested in iron-rich media, suggesting that compounds are iron-dependent antibiotics, unlike rifampicin, which showed the same MIC values in both iron-rich and iron-depleted media. To further investigate the contribution of the siderophore moiety and its role in exploiting the bacterial iron uptake system, we assessed the activity of **33** in the presence and absence

of the natural siderophore enterobactin (prepared following a previously published procedure with slight modifications, as illustrated in **Scheme S4**).[48-51] Under these conditions, we tested several *E. coli* strains, including wild-type BW 25113 as well as knockout strains *ΔentA* (impaired enterobactin biosynthesis), *ΔentC* (impaired enterobactin biosynthesis), and *ΔfepA* (impaired enterobactin import), and a standard *A. baumannii* ATCC 19606 strain (**Table 4**). In all cases, enterobactin supplementation reduced the activity of compound **33**. These results are in line with similar competition experiments performed for other siderophore conjugates and suggest that the uptake is likely mediated via a siderophore uptake route.[52-54] In the presence of enterobactin, conjugate **33** showed up to a 16-fold decrease in activity, while the potency of rifampicin remained unaffected. Taken together, these findings suggest that conjugate **33** operates by hijacking the bacterial cell's iron transport system to gain entry to the cell, after which the rifampicin moiety can engage with its target, eliciting its antibacterial effect. We also attempted to identify the specific transporter related to the increased activity of conjugate **33**. To do so, we tested **33** alongside rifampicin against a number of single knockout *E. coli* mutants, with impaired enterobactin (catecholate-type siderophore) transport (*ΔfepA, ΔfepB, ΔfepD*) or impaired ferrichrome (hydroxamate-type siderophore) transport *(ΔfhuA, ΔfhuB, ΔfhuC, ΔfhuD, ΔfhuE, ΔfhuF*).[55,56] The data obtained (**Table S1**) show no change in MIC for either compound **33** or rifampicin, when compared to the data against wild-type *E. coli*, suggesting that none of the transporters here assessed is singularly responsible for the increased activity of the conjugate **33**.

Table 4. MICs of compound **33** and rifampicin in ID-CAMHB (iron-poor medium) with and without enterobactin supplementation.

Strain	**MIC (μg/mL)**			
	33		Rifampicin	
	without enterobactin	+ 8 μg/mL enterobactin	without enterobactin	+ 8 μg/mL enterobactin
E. coli BW 25113	2	16	8	8
E. coli ΔentA	2	16	8	8
E. coli ΔentC	1	16	8	8
E. coli ΔfepA	2	8	8	8
A. baumannii ATCC 19606	0.5	4	2	2

Conclusions

In conclusion, we here report the development of a series of rifampicin-siderophore conjugates with activity against Gram-negative bacteria, which are normally impervious to the parent antibiotic. Our findings demonstrate that the activity of the conjugates is heavily dependent on the nature and length of the linkers used in conjugating rifampicin with established catechol-based iron-binding moieties. Notably, while the application of alkyne/azide click-chemistry successfully enabled the construction of a first-generation

rifampicin-siderophore conjugate, it was found to be devoid of activity, an effect subsequently attributed to the presence of the resulting triazole moiety. As an alternative, we found that rifampicin analogues prepared via ester conjugation showed improved activity compared to the parent antibiotic. Control experiments carried out with the natural siderophore enterobactin, as well as with iron-poor and iron-rich media, suggest that these conjugates exploit the bacterial cell's iron transport system to penetrate the OM. These findings serve to further inform the design of antibiotics aimed at leveraging bacteria's dependence on iron uptake pathways. Moreover, the synthetic routes developed for the preparation of rifampicin conjugates may open new avenues for further modifying the structure of this important antibiotic. Collectively, the results presented here contribute to the ongoing search for innovative antibacterial strategies in the fight against multidrug-resistant pathogens.

Acknowledgement

We thank Dr. Antoni Hendrickx from the Dutch National Institute for Public Health and the Environment (RIVM) for providing colistin-resistant bacteria isolates *E. coli* pRIVM_C029515_2 and *K. pneumoniae* RIVM_C019741. Financial support was provided by the Chinese Scholarship Council (CSC) in the form of a PhD Scholarship to M-L.G. (CSC file number 202207720043) and the Netherlands Organization for Scientific Research (NWO) through OTP grant no. 19384 to N.I.M.

Materials and methods

General information

Extended supporting information, which includes NMR and HPLC figures, is available free of charge at https://doi.org/10.1021/acsinfecdis.5c00311.

Reagents

All reagents employed were of American Chemical Society (ACS) grade or higher and were used without further purification unless otherwise stated.

HRMS

High-resolution mass spectra (HRMS) analyses were performed on a Shimadzu Nexera X2 UHPLC system with a Waters Acquity HSS C18 column (2.1 × 100 mm, 1.8 μm) at 30 °C and equipped with a diode array detector. The following solvent system, at a flow rate of 0.5 mL/min, was used: solvent A, 0.1 % formic acid in water; solvent B, 0.1 % formic acid in acetonitrile. Gradient elution was as follows: 95:5 (A/B) for 1 min, 95:5 to 15:85 (A/B) over 10 min, 15:85 to 0:100 (A/B) over 1 min, 0:100 (A/B) for 4 min, then reversion back to 95:5 (A/B) for 3 min. This system was connected to a Shimadzu 9030 QTOF mass spectrometer (ESI ionization), calibrated internally with Agilent's API-TOF reference mass solution kit (5.0 mM purine, 100.0 mM ammonium trifluoroacetate, and

2.5 mM hexakis(1*H*,1*H*,3*H*-tetrafluoropropoxy)phosphazine) diluted to achieve a mass count of 10000.

Analytical HPLC

HPLC analyses were performed on a Shimadzu Prominence-i LC-2030 system with a Dr. Maisch ReproSil Gold 120 C18 column (4.6 × 250 mm, 5 µm) at 30 °C and equipped with a UV detector monitoring at 214 and 254 nm. The following solvent system, at a flow rate of 1 mL/min, was used: solvent A, 0.1 % TFA in water/acetonitrile 95/5; solvent B, 0.1 % TFA in water/acetonitrile 5/95. Gradient elution was as follows: 100:0 (A/B) for 3 min, 100:0 to 0:100 (A/B) over 47 min, 0:100 (A/B) for 4 min, then reversion back to 100:0 (A/B) over 1 min, 100:0 (A/B) for 5 min.

Preparative HPLC

Method A

The compounds were purified using a BESTA-Technik system with a Dr. Maisch Reprosil Gold 120 C18 column (25 × 250 mm, 10 µm) and equipped with an ECOM Flash UV detector monitoring at 214 nm. At a flow rate of 12 mL/min, the following solvent system was used: solvent A, 0.1 % TFA in water/acetonitrile 95:5; solvent B, 0.1 % TFA in water/acetonitrile 5:95. Gradient elution was as follows: 100:0 (A/B) for 3 min, 100:0 to 40:60 (A/B) over 47 min, 40:60 to 0:100 (A/B) over 1 min, 0:100 (A/B) for 4 min, then reversion back to 100:0 (A/B) over 1 min, 100:0 (A/B) for 4 min. The fractions were analyzed, combined, and lyophilized to obtain purified compounds.

Method B

The compounds were purified using a BESTA-Technik system with a Dr. Maisch Reprosil Gold 120 C18 column (25 × 250 mm, 10 µm) and equipped with an ECOM Flash UV detector monitoring at 214 nm. At a flow rate of 12 mL/min, the following solvent system was used: solvent A, 0.1 % TFA in water/acetonitrile 95:5; solvent B, 0.1 % TFA in water/acetonitrile 5:95. Gradient elution was as follows: 80:20 (A/B) for 3 min, 80:20 to 0:100 (A/B) over 47 min, 0:100 (A/B) for 5 min, then reversion back to 80:20 (A/B) over 1 min, 80:20 (A/B) for 4 min. The fractions were analyzed, combined, and lyophilized to obtain purified compounds.

NMR

^{1}H and ^{13}C NMR spectra were recorded on Bruker AV 400 MHz (at 400 (^{1}H), and 101 (^{13}C) MHz), AV 600 MHz (at 600 (^{1}H), and 151 (^{13}C) MHz). The temperature of the NMR experiments was 298K unless stated otherwise. Chemical shifts are reported in ppm (δ) and were calibrated using residual deuterated solvent as an internal reference. (δ ^{1}H NMR: $CDCl_3$ 7.26; DMSO 2.50; δ ^{13}C NMR: $CDCl_3$ 77.16; DMSO 39.52). The NMR data are processed as follows: chemical shift, multiplicity (br s = broad singlet, s = singlet, d = doublet, dd = doublet of doublets, t = triplet, dt = doublet of triplets, q = quartet, tt = triplet

of triplets, m = multiplet), integration, coupling constants (*J*, reported in Hz) and a number of nuclei. NMR spectra were analyzed and processed using MestreNova version 14.2.0.

Antibacterial assay against Gram-negative and Gram-positive bacteria

From glycerol stocks, bacterial strains were cultured on blood agar plates and incubated overnight at 37 °C. Following incubation, 3 mL of tryptic soy broth (TSB) was inoculated with an individual colony. The cultures were grown to exponential phase (OD_{600nm} = 0.5) at 37 °C. The bacterial suspensions were then diluted 100-fold in CAMHB or ID-CAMHB to reach a bacterial cell density of 10^6 CFU mL^{-1}. In polypropylene 96-well microtiter plates, test compounds in assay media (e.g., CAMHB or ID-CAMHB) were added in triplicate and two-fold serially diluted to achieve a final volume of 50 µL per well. An equal volume of bacterial suspension (50 µL, 10^6 CFU mL^{-1}) was added to the wells. The plates were sealed with breathable membranes and incubated at 37 °C for 18-22 h with constant shaking (600 rpm). The MICs were determined by visual inspection as the median of a minimum of triplicates.

ID-CAMHB was prepared as follows: one liter of autoclaved MHB was incubated with 100 g of cation-binding resin Chelex 100 to remove cations, including iron, from the medium and filtered, and the pH was adjusted to 7.3 with hydrochloric acid. The medium was filtered again and supplemented with 20 to 25 mg/L of Ca^{2+} and 10 to 12.5 mg/L of Mg^{2+}, according to CLSI recommendations.

Hemolysis Assay

The hemolytic activity of compounds was assessed in triplicate. Red blood cells from defibrillated sheep blood obtained from Thermo Fisher were centrifuged (400 g for 15 min at 4 °C) and washed with phosphate-buffered saline (PBS) containing 0.002% Tween20 (buffer) five times. Then, the red blood cells were normalized to obtain a positive control read-out of 2.5 at 415 nm to stay within the linear range with the maximum sensitivity. A serial dilution of the compounds (64 to 2 µg/mL, 75 µL) was prepared in a 96-well plate. The outer border of the plate was filled with 75 µL buffer, the plate also contained a positive control (0.1% Triton-X final concentration, 75 µL) and a negative control (buffer, 75 µL) in triplicate. The normalized blood cells (75 µL) were added, and the plates were incubated at 37 °C for 1 h while shaking at 500 rpm. A flat-bottom polystyrene plate with 100 µL of buffer in each well was prepared. After incubation, the plate was centrifuged (800 g for 5 min at RT), and 25 µL of the supernatant was transferred to their respective wells in the flat-bottom plate. The values obtained from a read-out at 415 nm were corrected for background (negative control) and expressed as a percentage relative to the positive control (0.1% Triton-X).

Synthesis methods and analytical data

Rifampicin alkyne **2** was synthesized following previously published methods with minor changes**.** Spectral data obtained for all intermediates and rifampicin alkyne itself are in agreement with those reported in the literature.[39,40]

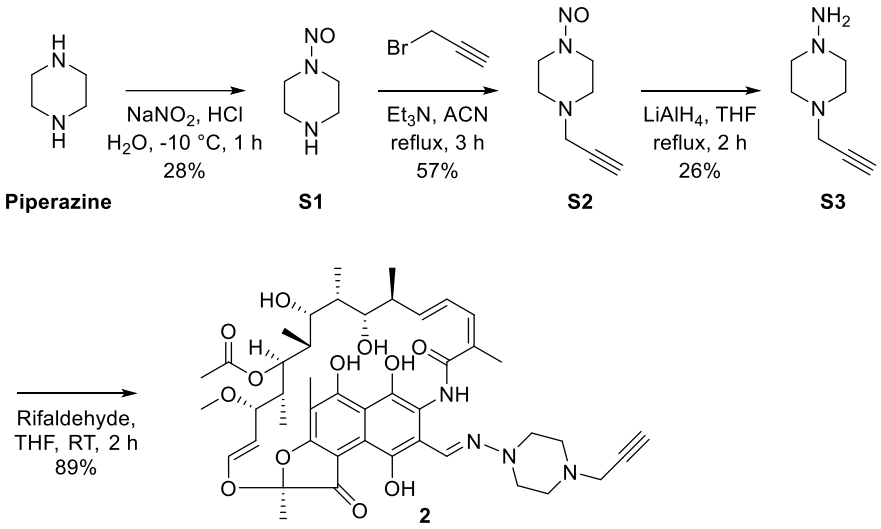

Scheme S1. Synthesis of Rifampicin alkyne **2**

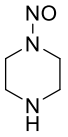

1-nitrosopiperazine (S1). Piperazine (5.16 g, 60 mmol) was dissolved in 6 M HCl (36 mL) and cooled to -10 °C. A solution of $NaNO_2$ (4.14 g, 60 mmol) in H_2O (72 mL) was added slowly by an addition funnel over 2 hours. The reaction mixture was adjusted to pH 10 with 3 M NaOH and extracted with DCM (3 × 100 mL). The combined organic extracts were dried over anhydrous Na_2SO4, concentrated in vacuo, and purified by flash column chromatography (SiO_2, 5% MeOH in DCM) to yield the compound **S1** as a yellow oil (1.98 g, 28%).

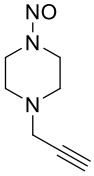

1-nitroso-4-propargylpiperazine (S2). 1-Nitrosopiperazine (**S1**) (1.2 g, 10.42 mmol) and propargyl bromide (1.16 mL of 80% solution in toluene, 10.42 mmol) were dissolved in dry MeCN (30 mL) and Et_3N (2.91 mL, 20.85 mmol). The reaction mixture was stirred at 75 °C for 3 hours and concentrated in vacuo. The crude was then dissolved in 10% NaOH (100 mL) and extracted with DCM (3 × 60 mL). The organic phase was dried over anhydrous Na_2SO_4, concentrated in vacuo, and purified by column chromatography (SiO_2, EtOAc/PE= 2:1) to yield the compound **S2** as an orange oil (900 mg, 57%).

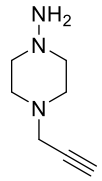

1-amino-4-propargylpiperazine (S3). 1-Nitroso-4-propargylpiperazine (**S2**) was dissolved in dry THF and cooled to 0 °C. $LiAlH_4$ (1 M in THF, 6.00 mL, 2.94 mmol) was added slowly and was stirred at 35 °C for 2 hours. The reaction mixture was then cooled, quenched with 2 M HCl (5 mL), and filtered through celite. The celite was subsequently washed with 2 M HCl (3 × 10 mL), and the filtrate was adjusted to pH 10 with 10% aq. NaOH. The aqueous phase was extracted with 3:1 $CHCl_3$/i-PrOH (4 × 350 mL), and the organic phase dried over anhydrous Na_2SO_4 and concentrated in vacuo. The crude product was purified by column chromatography (SiO_2, 10% MeOH in DCM) to yield the alkyne **S3** as an off-white solid (107 mg, 26%). **^{1}H NMR** (400 MHz, $CDCl_3$) δ 3.30 (d, J = 2.5 Hz, 2H), 3.02 (s, 2H), 2.65 (s, 6H), 2.25 (t, J = 2.4 Hz, 1H). **^{13}C{^{1}H} NMR** (101 MHz, $CDCl_3$) δ 78.7, 73.4, 59.3, 51.8, 46.6.

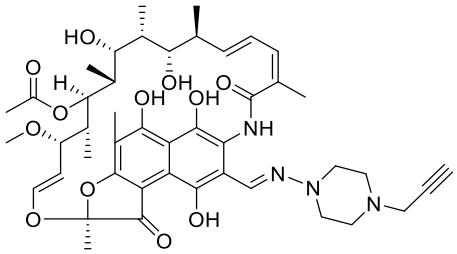

Rifampicin alkyne (2). Rifaldehyde (130 mg, 0.18 mmol) and 1-amino-4-propargylpiperazine (**S3**) (30 mg, 0.21 mmol) were dissolved in dry THF (3 mL), and the mixture was stirred vigorously for 2 hours. The mixture was then diluted with DCM (8 mL) and washed with 8 mL of a solution of ascorbic acid (2 g) in 3:1 H_2O/brine (40 mL). The aqueous phase was then extracted with DCM (2 × 8 mL), and the combined DCM extracts were dried over anhydrous Na_2SO_4 and concentrated in vacuo to yield rifampicin alkyne **2** as a red solid (136 mg, 89%). **^{1}H NMR** (400 MHz, $CDCl_3$) δ 12.04 (s, 1H), 8.30 (s, 1H), 6.64 – 6.52 (m, 1H), 6.39 (d, J = 11.1 Hz, 1H), 6.21 (dd, J = 12.7, 1.1 Hz, 1H), 5.94 (dd, J = 15.5, 5.0 Hz, 1H), 5.10 (dd, J = 12.7, 6.8 Hz, 1H), 4.94 (d, J = 10.6 Hz, 1H), 3.78 (s, 1H), 3.61 (d, J = 4.9 Hz, 1H), 3.51 – 3.44 (m, 2H), 3.42 (s, 1H), 3.23 (s, 1H), 3.14 (s, 1H), 3.04 (s, 3H), 3.03 – 2.99 (m, 1H), 2.77 (s, 2H), 2.38 (d, J = 7.0 Hz, 1H), 2.32 (s, 1H), 2.23 (s, 3H), 2.07 (d, J = 7.5 Hz, 6H), 1.80 (s, 3H), 1.74 – 1.68 (m, 1H), 1.59 – 1.50 (m, 1H), 1.41 – 1.31 (m, 1H), 1.02 (d, J = 7.0 Hz, 3H), 0.89 (d, J = 7.0 Hz, 3H), 0.60 (d, J = 6.9 Hz, 3H), -0.31 (d, J = 6.9 Hz, 3H). **HRMS** (ESI) *m/z*: $[M+H]^+$ calcd for $C_{45}H_{58}N_4O_{12}+H^+$: 847.4124; found: 847.4134.

Synthesis of azide-containing building blocks

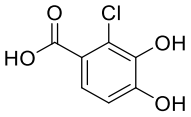

2-chloro-3,4-dihydroxybenzoic acid (6). Into a solution of 2-chloro-3,4-dimethoxybenzoic acid (**5**) (2 g, 9.23 mmol) in DCM (30 mL) was added a 1 M solution of BBr_3 in DCM (36.93 mL, 36.93 mmol) over 10 min at 0°C under Ar. After that, the reaction mixture was allowed to warm up to RT and was left stirring for an additional 3 h before it was poured into cold 2 M HCl (100 mL) and then extracted with EtOAc (2 × 100 mL). The organic layers were combined and washed with H_2O (100 mL), brine (50 mL), dried over Na_2SO_4, and concentrated in vacuo to give compound **6** (1.63 g, 94% yield). **^{1}H NMR** (400 MHz, DMSO-*d6*) δ 12.65 (br s, 1H), 10.41 (s, 1H), 9.31 (br s, 1H), 7.23 (d, *J* = 8.5 Hz, 1H),

6.76 (d, *J* = 8.5 Hz, 1H). **$^{13}C\{^1H\}$ NMR** (101 MHz, DMSO-*d6*) δ 166.6, 149.6, 142.6, 122.5, 121.6, 120.3, 112.8. **HRMS** (ESI) *m/z*: $[M-H]^-$ calcd for $C_7H_5ClO_4$-H^+: 186.9803; found: 186.9805.

CAUTION! Azides with a high Nitrogen/Carbon ratio can be explosive.

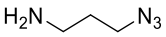

3-azidopropan-1-amine (4). To a solution of 3-chloropropan-1-amine hydrochloride salt (**3**) (3 g, 23.1 mmol) in water (15 mL) was added NaN_3 (4.5 g, 69.3 mmol), and the reaction was heated at 80 °C for 15 h. The solution was then basified with KOH (3.24 g, 57.8 mmol) and extracted with Et_2O (3 × 30 mL). The combined organic layers were dried over anhydrous Na_2SO_4, filtered, and the solvent was removed in vacuo at 25°C to give compound **4** (1.8 g, 78% yield) as a colorless oil. **^1H NMR** (400 MHz, $CDCl_3$) δ 3.38 (t, *J* = 6.7 Hz, 1H), 2.82 (t, *J* = 6.8 Hz, 1H), 1.74 (p, *J* = 6.8 Hz, 1H), 1.26 (br. s, 2H). Spectral data are in agreement with those reported in the literature.[57-59]

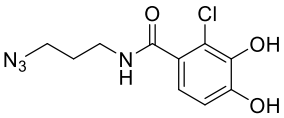

N-(3-azidopropyl)-2-chloro-3,4-dihydroxybenzamide (7). Into a solution of 3-azidopropan-1-amine (**4**) (265 mg, 2.65 mmol) in DCM (10 mL) and DMF (5 mL) were added HOBt (447.1 mg, 2.92 mmol), DIPEA (810 µL, 4.64 mmol), 2-chloro-3,4-dihydroxybenzoic acid (**6**) (250 mg, 1.33 mmol) and EDC*HCl (559.8 mg, 2.92 mmol), respectively, at RT. After stirring for 4 h, the reaction mixture was diluted with EtOAc (50 mL) and washed with sat. NH_4Cl (10 mL) and brine. The organic phase was dried over Na_2SO_4 and concentrated in vacuo to obtain the crude, which was purified using the HPLC method B to afford compound **7** (248 mg, 69% yield) as a colorless oil. **^1H NMR** (400 MHz, DMSO-d_6) δ 9.89 (br s, 1H), 9.37 (br s, 1H), 8.21 (t, J = 5.7 Hz, 1H), 6.76 – 6.70 (m, 2H), 3.41 (t, *J* = 6.8 Hz, 2H), 3.23 (q, J = 6.4 Hz, 2H), 1.73 (p, J = 6.8 Hz, 2H). **$^{13}C\{^1H\}$ NMR** (101 MHz, DMSO-d_6) δ 166.9, 147.3, 142.1, 128.8, 118.8, 117.8, 113.1, 48.6, 36.4, 28.4. **HRMS** (ESI) *m/z*: $[M+H]^+$ calcd for $C_{10}H_{11}ClN_4O_3$+H^+: 271.0593; found: 271.0595.

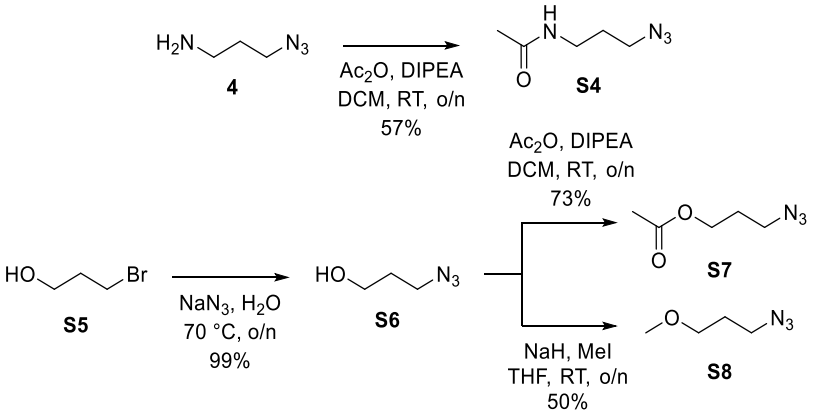

Scheme S2. Synthesis of the azide derivatives for the click-chemistry reaction with compound **2**.

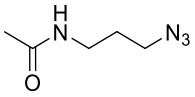

N-(3-azidopropyl)acetamide (S4). 3-Azidopropan-1-amine (**4**) (100 mg, 1 mmol) was dissolved in DCM (3 mL), and then DIPEA (174 µL, 1 mmol) was added, followed by Ac_2O (94.5 µL, 1 mmol), and the reaction was left stirring overnight under an Ar atmosphere. The next day, the solution was diluted with 1 M HCl (5 mL) and extracted with DCM (5 mL). The organic layer was washed with 1 M $NaHCO_3$ (5 mL), water (5 mL), and brine (5 mL), then dried over Na_2SO_4 and concentrated in vacuo at 25°C to obtain compound **S4** (81 mg, 57% yield) that was used as a substrate in the click-chemistry reaction without further purification. **^{1}H NMR** (400 MHz, $CDCl_3$) δ 5.74 (br s, 1H), 3.40 – 3.28 (m, 4H), 1.98 (s, 3H), 1.85 – 1.70 (m, 2H). Spectral data are in agreement with those reported in the literature.[60,61]

3-azidopropan-1-ol (S6). To a solution of 3-bromopropan-1-ol (**S5**) (3 g, 21.6 mmol) in water (15 mL) was added NaN_3 (4.21 g, 64.7 mmol), and the reaction was heated at 80 °C for 15 h. The reaction mixture was then extracted with Et_2O (3 × 30 mL). The combined organic layers were dried over anhydrous Na_2SO_4, filtered, and the solvent was removed in vacuo at 25°C to give compound **S6** (2.2 g, 99% yield) as a yellow oil. **^{1}H NMR** (400 MHz, $CDCl_3$) δ 3.76 (t, J = 6.0 Hz, 2H), 3.46 (t, J = 6.6 Hz, 2H), 1.84 (p, J = 6.4 Hz, 2H), 1.61 (s, 1H). Spectral data are in agreement with those reported in the literature.[62-64]

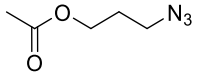

3-azidopropyl acetate (S7). 3-Azidopropan-1-ol (**S6**) (100 mg, 0.99 mmol) was dissolved in DCM (3 mL), and then DIPEA (172.3 µL, 0.99 mmol) was added, followed by Ac_2O (93.5 µL, 0.99 mmol), and the reaction was left stirring overnight under an Ar atmosphere. The next day, the solution was diluted with 1 M HCl (5 mL) and extracted with DCM (5 mL). The organic layer was washed with 1 M $NaHCO_3$ (5 mL), water (5 mL), and brine (5 mL), then dried over Na_2SO_4 and concentrated in vacuo at 25°C to obtain compound **S7** (104 mg, 73% yield) that was used as a substrate in the click-chemistry reaction without further purification.

^{1}H NMR (400 MHz, $CDCl_3$) δ 4.15 (t, *J* = 6.2 Hz, 2H), 3.39 (t, *J* = 6.7 Hz, 2H), 2.06 (s, 3H), 1.90 (p, *J* = 6.5 Hz, 2H). Spectral data are in agreement with those reported in the literature.[65]

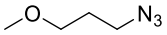

1-azido-3-methoxypropane (S8). 3-Azidopropan-1-ol (**S6**) (200 mg, 1.98 mmol) in THF (1 mL) was added dropwise to NaH (60% dispersion in mineral oil, 119 mg, 2.97 mmol) in DMF (3 mL) at 0 °C, and the reaction mixture was stirred for 30 min. After that, MeI (148 µL, 2.37 mmol) was added dropwise. The reaction mixture was allowed to warm to RT and then left stirring for an additional 3 h. The reaction was quenched by pouring into water (10 mL) and extracted with Et_2O (20 mL). The organic layer was washed with water (3 × 10 mL) and brine (10 mL), dried over anhydrous Na_2SO_4, filtered, and concentrated in vacuo at 25°C to obtain the compound **S8** (115 mg, 50% yield), which was used as a substrate in the click-chemistry reaction without further purification. **^{1}H NMR** (400 MHz, $CDCl_3$) δ 3.45 (t, *J* = 6.0 Hz, 2H), 3.38 (t, *J* = 6.7 Hz, 2H), 3.33 (s, 3H), 1.83 (p, *J* = 6.6 Hz, 2H). Spectral data are in agreement with those reported in the literature.[66,67]

5

Synthesis of triazole-linked conjugates 1, 8-12

General Procedure A (conditions for the conjugation using click-chemistry approach). The azide (0.04 mmol) and rifampicin alkyne (**2**) (0.02 mmol) were dissolved in 1:1 H_2O/tBuOH (650 µL). Freshly prepared aqueous solutions of ascorbic acid (500 mM, 85 µL, 0.04 mmol) and $CuSO_4 \cdot 5H_2O$ (100 mM, 100 µL, 0.01 mmol) were added, and the mixture was stirred at 50 °C for 2 h. After that, the reaction mixture was spiked with ascorbic acid (500 mM, 85 µL, 0.04 mmol), and then it was directly purified using the preparative HPLC method B. The fractions containing the pure product, as judged by HPLC, were combined and lyophilized to yield the corresponding triazole conjugates.

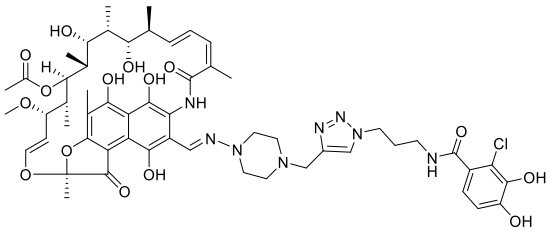

Conjugate 1. The compound was prepared according to General Procedure A, starting from rifampicin alkyne **2** (16.9 mg, 0.02 mmol) and azide **7** (110.8 mg, 0.04 mmol). Yield: 9 mg, 40%, orange powder.

HRMS (ESI) *m/z*: $[M+H]^+$ calcd for $C_{55}H_{69}ClN_8O_{15}+H^+$: 1117.4644; found: 1117.4633.

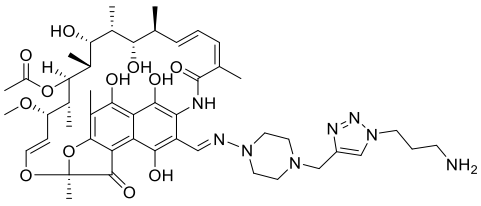

Conjugate 8. The compound was prepared according to General Procedure A, starting from rifampicin alkyne **2** (5 mg, 0.0059 mmol) and azide **4** (1.2 mg, 0.0118 mmol). Yield: 2.3 mg, 41%, orange powder.

HRMS (ESI) *m/z*: $[M+H]^+$ calcd for $C_{48}H_{66}N_8O_{12}+H^+$: 947.4873; found: 947.4864.

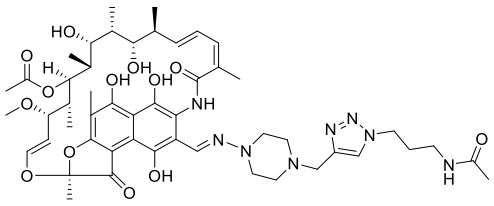

Conjugate 9. The compound was prepared according to General Procedure A, starting from rifampicin alkyne **2** (5 mg, 0.0059 mmol) and azide **S4** (1.7 mg, 0.0118 mmol). Yield: 2.5 mg, 43%, orange powder.

HRMS (ESI) *m/z*: $[M+H]^+$ calcd for $C_{50}H_{68}N_8O_{13}+H^+$: 989.4979; found: 989.4972.

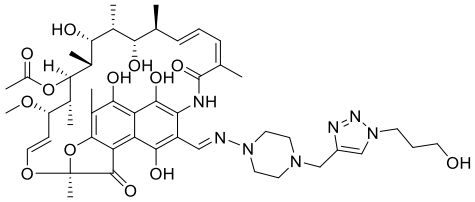

Conjugate 10. The compound was prepared according to General Procedure A, starting from rifampicin alkyne **2** (5 mg, 0.0059 mmol) and azide **S6** (1.2 mg, 0.0118 mmol). Yield: 2.6 mg, 47%, orange powder.

HRMS (ESI) *m/z*: $[M+H]^+$ calcd for $C_{48}H_{65}N_7O_{13}+H^+$: 948.4713; found: 948.4708.

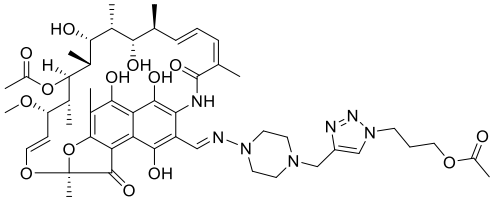

Conjugate 11. The compound was prepared according to General Procedure A, starting from rifampicin alkyne **2** (5 mg, 0.0059 mmol) and azide **S7** (1.7 mg, 0.0118 mmol). Yield: 2.3 mg, 39%, orange powder.

HRMS (ESI) *m/z*: $[M+H]^+$ calcd for $C_{50}H_{67}N_7O_{14}+H^+$: 990.4819; found: 990.4813.

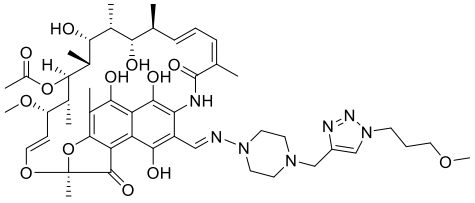

Conjugate 12. The compound was prepared according to General Procedure A, starting from rifampicin alkyne **2** (5 mg, 0.0059 mmol) and azide **S8** (1.4 mg, 0.0118 mmol). Yield: 2.4 mg, 42%, orange powder.

HRMS (ESI) *m/z*: $[M+H]^+$ calcd for $C_{49}H_{67}N_7O_{13}+H^+$: 962.4870; found: 962.4869.

Synthesis of benzyl-protected catechols

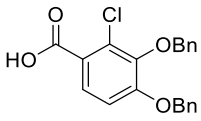

3,4-bis(benzyloxy)-2-chlorobenzoic acid (25). To a solution of 2-chloro-3,4-dihydroxybenzoic acid (**6**) (1.57 g, 8.33 mmol) and benzyl bromide (4.98 g, 29.1 mmol) in DMF (20 mL) was added pulverized K_2CO_3 (5.75 g, 41.6 mmol). After being stirred for 16 h, the reaction was quenched with 100 mL of distilled water and extracted with EtOAc (2 × 70 mL). The combined organic layers were washed with sat. NH_4Cl (70 mL), water (2 × 70 mL), and brine (50 mL), dried over anhydrous Na_2SO_4 and concentrated in vacuo. The obtained crude was then dissolved in the mixture of MeOH (30 mL), THF (10 mL), and 6 M aq. NaOH (10 mL) and was left stirring for 15 h at RT. After that, MeOH was evaporated, and the mixture was diluted with water (50 mL), washed with Et_2O (2 × 60 mL), and acidified with aq. HCl to form a white precipitate, which was filtered, washed with water (2 x 10 mL), petroleum ether (2 x 15 mL), and then dried to obtain compound **25** (2.85 g, 93% yield) as a white solid. **^{1}H NMR** (400 MHz, DMSO-*d6*) δ 13.09 (s, 1H), 7.65 (d, *J* = 8.8 Hz, 1H), 7.54 – 7.47 (m, 2H), 7.46 – 7.29 (m, 8H), 7.24 (d, *J* = 8.9 Hz, 1H), 5.26 (s, 2H), 4.97 (s, 2H). **^{13}C{^{1}H} NMR** (101 MHz, DMSO-*d6*) δ 166.1, 155.1, 144.3, 136.8, 136.2, 128.6, 128.5, 128.3, 128.2, 128.2, 128.0, 127.7, 127.2, 123.7, 112.0, 74.2, 70.4. **HRMS** (ESI) *m/z*: $[M+H]^+$ calcd for $C_{21}H_{17}ClO_4+H^+$: 369.0888; found: 369.0892.

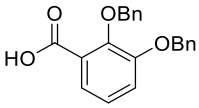

2,3-bis(benzyloxy)benzoic acid (26). To a solution of 2,3-dihydroxybenzoic acid (**24**) (5 g, 32.4 mmol) and benzyl bromide (19.4 g, 113.4 mmol) in DMF (40 mL), pulverized K_2CO_3 (22.4 g, 162 mmol) was added. After being stirred for 16 h, the reaction was quenched with 200 mL of water and extracted with EtOAc (2 × 150 mL). The combined organic layers were washed with sat. NH_4Cl (150 mL), water (2 × 150 mL), and brine (100 mL), dried over anhydrous Na_2SO_4 and concentrated in vacuo. The obtained crude was then dissolved in the mixture of MeOH (150 mL), THF (20 mL), and 6 M aq. NaOH (30 mL) and was left stirring for 15 h at RT. After that, MeOH was evaporated, and the mixture was diluted with water (100 mL), washed with Et_2O (2 × 60 mL), and acidified with aq. HCl to form a white precipitate, which was filtered, washed with water (2 × 20 mL), petroleum ether (2 × 30 mL), and then dried to obtain compound **26** (10.2 g, 94% yield) as a white solid. **^{1}H NMR** (400 MHz, DMSO-*d6*) δ 12.95 (br s, 1H), 7.53 – 7.46 (m, 2H), 7.44 – 7.25 (m, 9H), 7.25 – 7.11 (m, 2H), 5.19 (s, 2H), 5.00 (s, 2H). **^{13}C{^{1}H} NMR** (101 MHz, DMSO-*d6*) δ 167.5, 152.3, 146.6, 137.5, 136.8, 128.5, 128.2, 128.1, 128.0, 127.8, 127.8, 124.2, 121.5, 117.0, 74.7, 70.2. **HRMS** (ESI) *m/z*: $[M+H]^+$ calcd for $C_{21}H_{18}O_4+H^+$: 335.1278; found: 335.1282.

Synthesis of piperazine-containing building blocks

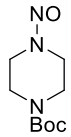

***tert*-butyl 4-nitrosopiperazine-1-carboxylate (14).** *tert*-Butyl piperazine-1-carboxylate (**13**) (10 g, 53.69 mmol) and *tert*-butyl nitrite (13.84 g, 134.23 mmol) were mixed together in a round-bottom flask, and the mixture was left stirring at 50°C under an Ar atmosphere for 24 h. After that, the excess of *tert*-butyl nitrite was evaporated under reduced pressure to obtain compound **14** (11.56 g, quantitative yield) as yellow crystals. **^{1}H NMR** (400 MHz, $CDCl_3$) δ 4.28 – 4.21 (m, 2H), 3.83 – 3.76 (m, 2H), 3.70 – 3.63 (m, 2H), 3.47 – 3.40 (m, 2H), 1.47 (s, 9H). **^{13}C{^{1}H} NMR** (101 MHz, $CDCl_3$) δ 154.4, 81.0, 49.4, 39.8, 28.4. **HRMS** (ESI) *m/z*: $[M+H]^+$ calcd for $C_9H_{17}N_3O_3+H^+$: 216.1343; found: 216.1346. Spectral data are in agreement with those reported in the literature.[68]

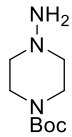

***tert*-butyl 4-aminopiperazine-1-carboxylate (15).** To a stirred solution of *tert*-butyl 4-nitrosopiperazine-1-carboxylate (**14**) (16 g, 74.33 mmol) in THF/H_2O (1:1, 500 mL), NH_4Cl (64 g, 1.19 mol) was added, followed by portion-wise addition of Zn dust (39 g, 0.59 mol). After the addition was completed, the reaction mixture was left stirring at RT overnight. After that, the reaction mixture was filtered, and the filtrate was extracted with MTBE (2 × 300 mL). Organic layers were combined, washed with brine (100 mL), dried over anhydrous Na_2SO_4, and concentrated under reduced pressure to obtain compound **15** (7.18 g, 48% yield) as a white solid. **^{1}H NMR** (400 MHz, $CDCl_3$) δ 3.46 (br s, 4H), 3.05 (br s, 2H), 2.55 (br s, 4H), 1.44 (s, 9H). **^{13}C{^{1}H} NMR** (101 MHz, $CDCl_3$) δ 154.7, 80.0, 59.2, 46.0, 28.5. **HRMS** (ESI) *m/z*: $[M+H]^+$ calcd for $C_9H_{19}N_3O_2+H^+$: 202.1550; found: 202.1553.

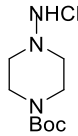

***tert*-butyl 4-(((benzyloxy)carbonyl)amino)piperazine-1-carboxylate (16).** To a stirred solution of *tert*-butyl 4-aminopiperazine-1-carboxylate (**15**) (6.34 g, 31.5 mmol) in THF (120 mL) was added Et_3N (8.78 mL, 63 mmol), followed by dropwise addition of CbzCl (4.5 mL, 31.5 mmol). After the addition was completed, the reaction mixture was left stirring at RT overnight. After that, the reaction mixture was diluted with water (100 mL) and extracted with MTBE (200 mL). The organic layer was separated, washed with water (100 mL) and brine (50 mL), dried over anhydrous Na_2SO_4, and concentrated under reduced pressure. The residue was triturated with petroleum ether (50 mL) and filtered. The precipitate was washed with petroleum ether (2 × 30 mL) and dried to obtain compound **16** (9.17 g, 87% yield) as white crystals. **^{1}H NMR** (400 MHz, $CDCl_3$) δ 7.41 – 7.27 (m, 5H), 5.74 (br s, 1H), 5.13 (s, 2H), 3.57 – 3.50 (m, 4H), 2.79 – 2.72 (m, 4H), 1.45 (s, 9H). **^{13}C{^{1}H} NMR** (101 MHz, $CDCl_3$) δ 154.6, 136.2, 128.7, 128.4, 80.2, 67.2, 56.0, 55.7, 43.3, 28.5. **HRMS** (ESI) *m/z*: $[M+H]^+$ calcd for $C_{17}H_{25}N_3O_4+H^+$: 336.1918; found: 336.1930.

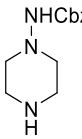

benzyl piperazin-1-ylcarbamate (17). TFA (15 mL) was added to a stirred solution of *tert*-butyl 4-(((benzyloxy)carbonyl)amino)piperazine-1-carboxylate (**16**) (9.1 g, 27.13 mmol) in DCM (15 mL), and the mixture was left stirring for 1 h. The volatile solvents were evaporated, and the residue

was triturated with MTBE (30 mL) to obtain the precipitate, which was filtered, washed with MTBE (2 × 30 mL), and dried to give the compound **17** (3.32 g, 52% yield, calculated for 2 × TFA counterions) as a white powder. **^{1}H NMR** (400 MHz, DMSO-d_6) δ 9.03 (br s, 2H), 8.90 (br s, 1H), 7.41 – 7.27 (m, 5H), 5.03 (s, 2H), 3.19 – 3.12 (m, 4H), 3.01 – 2.89 (m, 4H). **^{13}C{^{1}H} NMR** (101 MHz, DMSO-d_6) δ 154.8, 136.9, 128.5, 128.0, 127.9, 65.5, 51.3, 42.8. **HRMS** (ESI) *m/z*: $[M+H]^+$ calcd for $C_{12}H_{17}N_3O_2$+H^+: 236.1394; found: 236.1399.

General Procedure B (alkylation of piperazines). Bromoalcohol (4.32 mmol) was added to a stirred suspension of piperazine **17** (1 g, 2.16 mmol) and K_2CO_3 (1.5 g, 10.79 mmol) in MeCN (15 mL), and the mixture was left stirring at 80°C overnight. The next day, the solvent was evaporated, and the residue was redissolved in water (30 mL), followed by extraction with EtOAc (2 × 30 mL). The combined organic layers were washed with brine (15 mL), dried over anhydrous Na_2SO_4, and concentrated under reduced pressure. The residue was triturated with petroleum ether (10 mL) and filtered. The precipitate was washed with petroleum ether (2 × 10 mL) and dried to obtain the product.

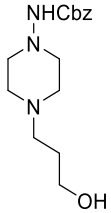

benzyl (4-(3-hydroxypropyl)piperazin-1-yl)carbamate (18). The compound was prepared according to General Procedure B, starting from piperazine **17** (1 g, 2.16 mmol) and 3-bromo-1-propanol (0.6 g, 4.32 mmol). Yield: 0.42 g, 66%, white powder. For analytical purposes, the compound was purified via the preparative HPLC method A. NMR data are provided for the TFA salt. **^{1}H NMR** (400 MHz, DMSO-d_6) δ 9.75 (br s, 1H), 8.89 (br s, 1H), 7.42 – 7.27 (m, 5H), 5.04 (s, 2H), 3.46 (t, J = 5.9 Hz, 4H), 3.16 – 2.90 (m, 8H), 1.82 – 1.71 (m, 2H). **^{13}C{^{1}H} NMR** (101 MHz, DMSO-d_6) δ 154.7, 136.8, 128.4, 128.0, 127.9, 65.5, 58.0, 53.6, 51.2, 50.8, 26.7. **HRMS** (ESI) *m/z*: $[M+H]^+$ calcd for $C_{15}H_{23}N_3O_3$+H^+: 294.1812; found: 294.1826.

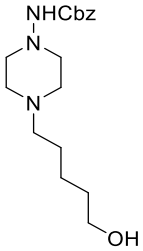

benzyl (4-(5-hydroxypentyl)piperazin-1-yl)carbamate (19). The compound was prepared according to General Procedure B, starting from piperazine **17** (1 g, 2.16 mmol) and 5-bromo-1-pentanol (0.72 g, 4.32 mmol). Yield: 0.48 g, 69%, white powder. For analytical purposes, the compound was purified via the preparative HPLC method A. NMR data are provided for the TFA salt. **^{1}H NMR** (400 MHz, DMSO-d_6) δ 9.63 (br s, 1H), 8.89 (br s, 1H), 7.42 – 7.27 (m, 5H), 5.04 (s, 2H), 3.46 (d, J = 11.5 Hz, 2H), 3.39 (t, J = 6.3 Hz, 2H), 3.15 – 2.90 (m, 8H), 1.67 – 1.54 (m, 2H), 1.48 – 1.37 (m, 2H), 1.37 – 1.23 (m, 2H). **^{13}C{^{1}H} NMR** (101 MHz, DMSO-d_6) δ 154.8, 136.8, 128.4, 128.0, 127.9, 65.5, 60.3, 55.4, 51.1, 50.7, 31.8, 23.2, 22.6. **HRMS** (ESI) *m/z*: $[M+H]^+$ calcd for $C_{17}H_{27}N_3O_3$+H^+: 322.2125; found: 322.2134.

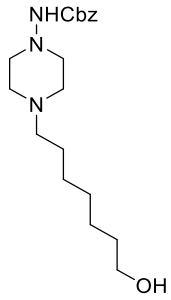

benzyl (4-(7-hydroxyheptyl)piperazin-1-yl)carbamate (20). The compound was prepared according to General Procedure B, starting from piperazine **17** (1 g, 2.16 mmol) and 7-bromo-1-heptanol (0.95 g, 4.32 mmol). Yield: 0.867 g, 79%, white powder. For analytical purposes, the compound was purified via the preparative HPLC method A. NMR data are provided for the TFA salt. **^{1}H NMR** (400 MHz, DMSO-d_6) δ 9.75 (br s, 1H), 8.89 (br s, 1H), 7.42 – 7.27 (m, 5H), 5.04 (s, 2H), 3.46 (d, J = 11.5 Hz, 2H), 3.37 (t, J = 6.5 Hz, 2H), 3.16 – 2.89 (m, 8H), 1.64 – 1.54 (m, 2H), 1.44 – 1.36 (m, 2H), 1.34 – 1.22 (m, 6H). **^{13}C{^{1}H} NMR** (101 MHz, DMSO-d_6) δ 154.8, 136.8, 128.4, 128.0, 127.9, 65.5, 60.6, 55.3, 51.2, 50.7, 32.4, 28.4, 26.0, 25.3, 23.3. **HRMS** (ESI) *m/z*: $[M+H]^+$ calcd for $C_{19}H_{31}N_3O_3+H^+$: 350.2438; found: 350.2457.

General Procedure C (esterification of catecholates with piperazine-containing alcohols). The alcohol (0.343 mmol) and the protected catechol (0.343 mmol) were mixed together in dry DCM prior to the addition of DIC (161 µL, 1.02 mmol) and DMAP (4.2 mg, 0.034 mmol). The obtained mixture was left stirring under an Ar atmosphere overnight. The following day, the solvent was evaporated, and the residue was extracted with water (10 mL) and MTBE (20 mL). The organic layer was separated, washed with sat. $NaHCO_3$ (10 mL), water (10 mL), brine (5 mL), dried over anhydrous Na_2SO_4, and concentrated under reduced pressure. The obtained crude was dissolved in THF (10 mL), followed by the addition of Pd/C (25 mg). The reaction mixture was left stirring overnight under an H_2 atmosphere (1 bar, balloon). The next day, the suspension was filtered, and the filtrate was concentrated in vacuo to obtain the desired product.

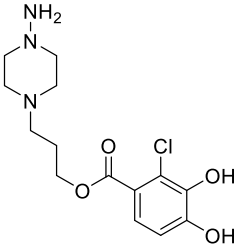

3-(4-aminopiperazin-1-yl)propyl 2-chloro-3,4-dihydroxybenzoate (27). The compound was prepared according to General Procedure C, starting from alcohol **18** (100 mg, 0.343 mmol) and catechol **25** (126 mg, 0.343 mmol). Yield: 52 mg, 46%, white powder. For analytical purposes, the compound was purified via the preparative HPLC method A. NMR data are provided for the TFA salt. **^{1}H NMR** (400 MHz, DMSO-d_6) δ 10.81 (br s, 1H), 9.84 (br s, 3H), 9.45 (br s, 1H), 7.29 (d, J = 8.5 Hz, 1H), 6.82 (d, J = 8.5 Hz, 1H), 4.25 (t, J = 5.9 Hz, 3H), 3.85 – 2.80 (m, 10H), 2.12 – 2.00 (m, 2H). **^{13}C{^{1}H} NMR** (101 MHz, DMSO-d_6) δ 164.8, 150.3, 142.8, 122.8, 120.3, 120.1, 112.9, 61.8, 52.8, 50.4, 50.2, 23.2. **HRMS** (ESI) *m/z*: $[M+H]^+$ calcd for $C_{14}H_{20}ClN_3O_4+H^+$: 330.1215; found: 330.1218.

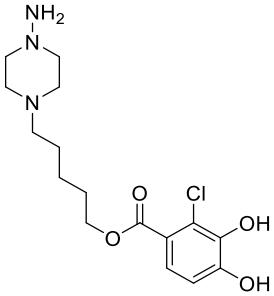

5-(4-aminopiperazin-1-yl)pentyl 2-chloro-3,4-dihydroxybenzoate (28). The compound was prepared according to General Procedure C, starting from alcohol **19** (110 mg, 0.343 mmol) and catechol **25** (126 mg, 0.343 mmol). Yield: 61 mg, 50%, white powder. For analytical purposes, the compound was purified via the preparative HPLC method A. NMR data are provided for the TFA salt. **^{1}H NMR** (400 MHz, DMSO-d_6) δ 10.76 (br s, 1H), 9.89 (br s, 3H), 9.44 (s, 1H), 7.22 (d, J = 8.5 Hz, 1H), 6.82 (d, J = 8.5 Hz, 1H), 4.19 (t, J = 6.3 Hz, 2H), 3.59 (br s, 2H), 3.32 (br s, 2H), 3.20 – 3.01 (m, 4H), 2.96 (s, 2H), 1.76 – 1.60 (m, 4H), 1.40 (p, J = 7.6 Hz, 2H). **^{13}C{^{1}H} NMR** (101 MHz, DMSO-d_6) δ 165.1, 150.1, 142.8, 122.4, 120.7, 120.1, 112.9, 64.1, 55.1, 50.2, 50.0, 27.6, 22.9, 22.6. **HRMS** (ESI) *m/z*: $[M+H]^+$ calcd for $C_{16}H_{24}ClN_3O_4+H^+$: 358.1528; found: 358.1537.

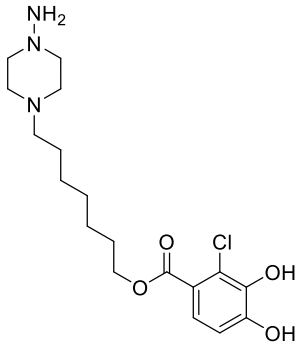

7-(4-aminopiperazin-1-yl)heptyl 2-chloro-3,4-dihydroxybenzoate (29). The compound was prepared according to General Procedure C, starting from alcohol **20** (120 mg, 0.343 mmol) and catechol **25** (126 mg, 0.343 mmol). Yield: 53 mg, 40%, white powder. For analytical purposes, the compound was purified via the preparative HPLC method A. NMR data are provided for the TFA salt. **^{1}H NMR** (400 MHz, DMSO-d_6) δ 10.71 (br s, 1H), 9.85 (br s, 3H), 9.43 (br s, 1H), 7.20 (d, J = 8.5 Hz, 1H), 6.81 (d, J = 8.5 Hz, 1H), 4.18 (t, J = 6.5 Hz, 2H), 3.55 (br s, 2H), 3.32 (br s, 2H), 3.19 – 3.00 (m, 4H), 2.95 (br s, 2H), 1.72 – 1.53 (m, 4H), 1.44 – 1.20 (m, 6H). **^{13}C{^{1}H} NMR** (101 MHz, DMSO-d_6) δ 165.2, 150.0, 142.7, 122.3, 120.8, 120.1, 112.9, 64.5, 55.2, 50.2, 50.0, 28.1, 28.0, 25.9, 25.3, 23.2. **HRMS** (ESI) *m/z*: $[M+H]^+$ calcd for $C_{18}H_{28}ClN_3O_4+H^+$: 386.1841; found: 386.1853.

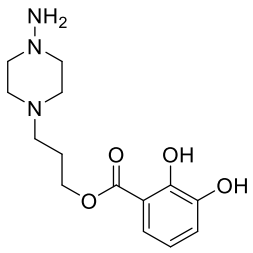

3-(4-aminopiperazin-1-yl)propyl 2,3-dihydroxybenzoate (30). The compound was prepared according to General Procedure C, starting from alcohol **18** (100 mg, 0.343 mmol) and catechol **26** (126 mg, 0.343 mmol). Yield: 14 mg, 14%, white powder. For analytical purposes, the compound was purified via the preparative HPLC method A. NMR data are provided for the TFA salt. **^{1}H NMR** (400 MHz, DMSO-d_6) δ 10.33 (s, 1H), 9.98 (br s, 1H), 9.65 (br s, 2H), 9.53 (br s, 1H), 7.27 (dd, J = 8.0, 1.6 Hz, 1H), 7.04 (dd, J = 7.8, 1.6 Hz, 1H), 6.75 (t, J = 7.9 Hz, 1H), 4.36 (t, J = 5.9 Hz, 2H), 3.41 – 3.04 (m, 8H), 2.92 (br s, 2H), 2.18 – 2.01 (m, 2H). **^{13}C{^{1}H} NMR** (101 MHz, DMSO-d_6) δ 169.2, 149.4, 146.1, 120.7, 119.8, 118.9, 113.3, 62.4, 52.7, 50.2, 23.1. **HRMS** (ESI) *m/z*: $[M+H]^+$ calcd for $C_{14}H_{21}N_3O_4+H^+$: 296.1605; found: 296.1612.

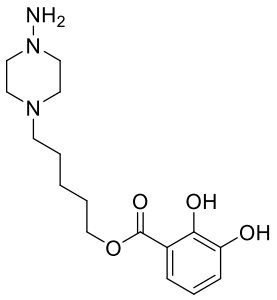

5-(4-aminopiperazin-1-yl)pentyl 2,3-dihydroxybenzoate (31). The compound was prepared according to General Procedure C, starting from alcohol **19** (110 mg, 0.343 mmol) and catechol **26** (114 mg, 0.343 mmol). Yield: 64 mg, 58%, white powder. For analytical purposes, the compound was purified via the preparative HPLC method A. NMR data are provided for the TFA salt. **^{1}H NMR** (400 MHz, DMSO-d_6) δ 10.46 (s, 1H), 9.92 (br s, 3H), 9.57 (br s, 1H), 7.23 (dd, J = 8.0, 1.6 Hz, 1H), 7.04 (dd, J = 7.8, 1.6 Hz, 1H), 6.74 (t, J = 7.9 Hz, 1H), 4.30 (t, J = 6.4 Hz, 2H), 3.58 (br s, 2H), 3.33 (br s, 2H), 3.2 – 3.05 (m, 4H), 2.96 (br s, 2H), 1.79 – 1.61 (m, 4H), 1.41 (p, J = 7.6 Hz, 2H). **^{13}C{^{1}H} NMR** (101 MHz, DMSO-d_6) δ 169.6, 149.6, 146.2, 120.8, 119.5, 119.0, 113.2, 64.7, 55.1, 50.2, 50.0, 27.5, 22.9, 22.5. **HRMS** (ESI) *m/z*: $[M+H]^+$ calcd for $C_{16}H_{25}N_3O_4+H^+$: 324.1918; found: 324.1928.

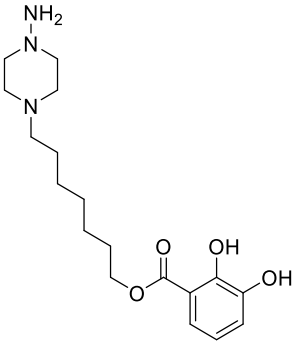

7-(4-aminopiperazin-1-yl)heptyl 2,3-dihydroxybenzoate (32). The compound was prepared according to General Procedure C, starting from alcohol **20** (120 mg, 0.343 mmol) and catechol **26** (114 mg, 0.343 mmol). Yield: 49 mg, 41%, white powder. For analytical purposes, the compound was purified via the preparative HPLC method A. NMR data are provided for the TFA salt. **^{1}H NMR** (400 MHz, DMSO-d_6) δ 10.48 (s, 1H), 9.86 (s, 3H), 9.52 (s, 1H), 7.22 (dd, J = 8.0, 1.6 Hz, 1H), 7.04 (dd, J = 7.8, 1.5 Hz, 1H), 6.75 (t, J = 7.9 Hz, 1H), 4.30 (t, J = 6.5 Hz, 2H), 3.57 (br s, 2H), 3.39 – 3.21 (m, 2H), 3.18 – 3.00 (m, 4H), 2.95 (br s, 2H), 1.71 (p, J = 6.6 Hz, 2H), 1.66 – 1.56 (m, 2H), 1.44 – 1.23 (m, 6H). **^{13}C{^{1}H} NMR** (101 MHz, DMSO-d_6) δ 169.6, 149.6, 146.2, 120.8, 119.4, 119.0, 113.1, 65.1, 55.2, 50.2, 50.0, 28.1, 27.9, 25.8, 25.2, 23.2. **HRMS** (ESI) *m/z*: $[M+H]^+$ calcd for $C_{18}H_{29}N_3O_4+H^+$: 352.2231; found: 352.2242.

Synthesis of amide S12

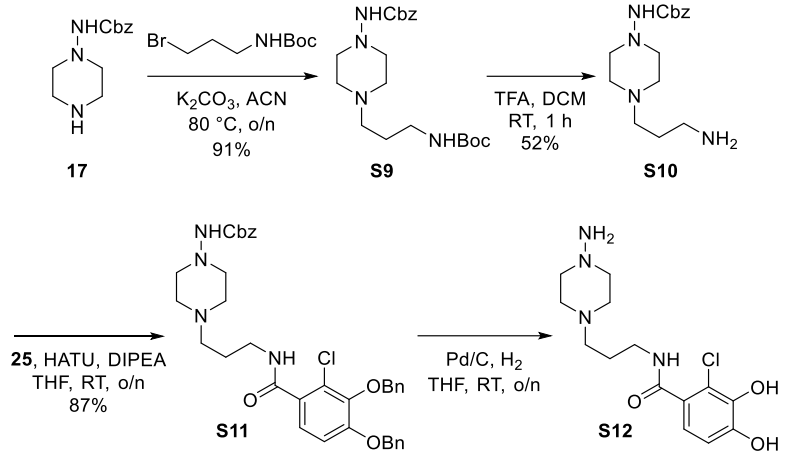

Scheme S3. Synthesis of the amide **S12**.

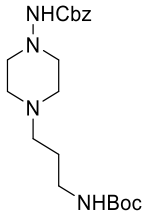

benzyl (4-(3-((*tert*-butoxycarbonyl)amino)propyl)piperazin-1-yl)-carbamate (S9). *tert*-Butyl (3-bromopropyl)carbamate (284 mg, 1.19 mmol) was added to a stirred suspension of piperazine **17** (500 mg, 1.08 mmol) and K_2CO_3 (750 mg, 5.40 mmol) in MeCN (10 mL), and the mixture was left stirring at 80°C overnight. The next day, the solvent was evaporated, and the residue was redissolved in water (20 mL), followed by extraction with MTBE (2 × 25 mL). The combined organic layers were washed with brine (15 mL), dried over anhydrous Na_2SO_4, and concentrated under reduced pressure. The residue was purified via column chromatography (SiO_2, DCM/MeOH/Et_3N = 99:1:0.1, R_f = 0.3) to afford compound **S9** (386 mg, 91% yield) as a white powder. **^{1}H NMR** (400 MHz, $CDCl_3$) δ 7.38 – 7.27 (m, 5H), 5.64 (br s, 1H), 5.26 (br s, 1H), 5.12 (s, 2H), 3.17 (q, *J* = 6.0 Hz, 2H), 2.83 (br s, 4H), 2.58 (br s, 4H), 2.42 (t, *J* = 6.8 Hz, 2H), 1.63 (p, *J* = 6.7 Hz, 2H), 1.42 (s, 9H). **^{13}C{^{1}H} NMR** (101 MHz, $CDCl_3$) δ 156.2, 136.3, 128.7, 128.4, 67.1, 56.3, 56.1, 52.4, 39.8, 28.6, 26.7. **HRMS** (ESI) *m/z*: $[M+H]^+$ calcd for $C_{20}H_{32}N_4O_4+H^+$: 393.2497; found: 393.2512.

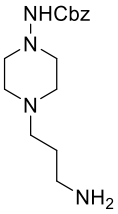

benzyl (4-(3-aminopropyl)piperazin-1-yl)carbamate (S10). TFA (5 mL) was poured into the solution of compound **S9** (386 mg, 0.985 mmol) in DCM (5 mL), and the reaction was left stirring at RT for 1 h. After that, the mixture was evaporated, and the residue was triturated with THF (5 mL) to obtain the precipitate, which was filtered and washed with MTBE (2 × 5 mL) to afford TFA salt of the compound **S10** (267 mg, 52% yield, calcd for 2×TFA salt) as a white powder. **^{1}H NMR** (400 MHz, DMSO-*d*$_6$) δ 10.13 (br s, 1H), 8.91 (br s, 1H), 8.01 (s, 3H), 7.42 – 7.27 (m, 5H), 5.04 (s, 2H), 3.54 – 3.34 (m, 2H), 3.22 – 2.77 (m, 10H), 1.92 (p, *J* = 8.3 Hz, 2H). **^{13}C{^{1}H} NMR** (101 MHz, DMSO-

d$_6$) δ 154.8, 136.8, 128.4, 128.0, 127.9, 65.5, 52.6, 51.2, 50.8, 36.3, 21.8. **HRMS** (ESI) *m/z*: $[M+H]^+$ calcd for $C_{15}H_{24}N_4O_2+H^+$: 293.1972; found: 293.1982.

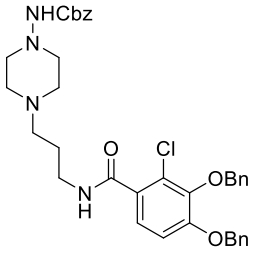

benzyl (4-(3-(3,4-bis(benzyloxy)-2-chlorobenzamido)-propyl)piperazin-1-yl)carbamate (S11). The amine **S10** (262 mg, 0.503 mmol), the protected catechol **25** (186 mg, 0.503 mmol), and DIPEA (880 µl, 5.03 mmol) were mixed together in dry DCM prior to the addition of HATU (191 mg, 0.503 mmol). The obtained mixture was left stirring under an Ar atmosphere overnight. The following day, the solvent was evaporated, and the residue was diluted with water (10 mL) and MTBE (10 mL) to form the precipitate, which was filtered, washed with MTBE (10 mL), PE (10 mL), and dried to afford compound **S11** (281 mg, 87% yield) as an off-yellow powder. **^{1}H NMR** (400 MHz, $CDCl_3$) δ 7.48 – 7.28 (m, 17H), 6.93 (d, *J* = 8.7 Hz, 1H), 5.52 (br s, 1H), 5.15 (s, 2H), 5.10 (s, 2H), 5.03 (s, 2H), 3.53 (q, *J* = 5.9 Hz, 2H), 2.88 – 2.54 (m, 8H), 2.51 (t, *J* = 6.3 Hz, 2H), 1.76 (p, *J* = 6.2 Hz, 2H). **^{13}C{^{1}H} NMR** (101 MHz, $CDCl_3$) δ 166.3, 154.3, 144.9, 136.9, 136.1, 129.4, 128.8, 128.7, 128.7, 128.5, 128.4, 128.4, 127.6, 126.2, 125.4, 112.3, 75.1, 71.1, 67.0, 56.8, 56.0, 52.4, 39.8, 25.5. **HRMS** (ESI) *m/z*: $[M+H]^+$ calcd for $C_{36}H_{39}ClN_4O_5+H^+$: 643.2682; found: 643.2702.

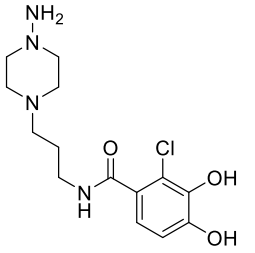

***N*-(3-(4-aminopiperazin-1-yl)propyl)-2-chloro-3,4-dihydroxbenzamide (S12)**. The amide **S11** (281 mg, 0.437 mmol) was dissolved in THF (20 mL), followed by the addition of Pd/C (50 mg). The reaction mixture was left stirring for 2 days under an H_2 atmosphere (1 bar, balloon). The next day, the suspension was filtered, and the filtrate was concentrated in vacuo to obtain compound **S12** (142 mg, 99% yield, unpurified) as a white powder that was used in the next step without further purification. **HRMS** (ESI) *m/z*: $[M+H]^+$ calcd for $C_{14}H_{21}ClN_4O_3+H^+$: 329.1375; found: 329.1378.

Synthesis of alcohols 21-23, ester-linked conjugates 33-38, and amide 39

General Procedure D (conjugation of piperazine-containing alcohols with rifaldehyde. The alcohol (0.028 mmol) was dissolved in THF (5 mL), followed by the addition of Pd/C (10 mg). The reaction mixture was left stirring overnight under an H_2 atmosphere (1 bar, balloon). The next day, the suspension was filtered, and the filtrate was concentrated and directly dissolved in THF (5 mL). Rifaldehyde (10 mg, 0.014 mmol) was added, and the resulting solution was left stirring for 2 h. After that, the reaction mixture was evaporated and then directly purified using the preparative HPLC method B. The fractions containing the pure product, as judged by HPLC, were combined and lyophilized to yield the desired product.

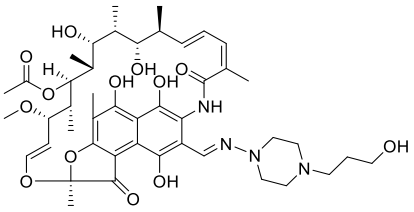

Compound 21. The compound was prepared according to General Procedure D, starting from alcohol **18** (4.5 mg, 0.028 mmol) and rifaldehyde (10 mg, 0.014 mmol). Yield: 3.4 mg, 28%, orange powder.

HRMS (ESI) *m/z*: $[M+H]^+$ calcd for $C_{45}H_{62}N_4O_{13}+H^+$: 867.4387; found: 867.4404.

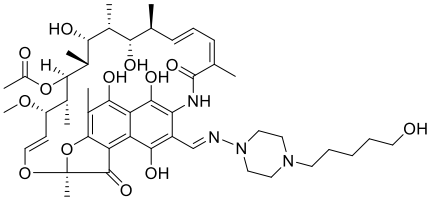

Compound 22. The compound was prepared according to General Procedure D, starting from alcohol **19** (5.3 mg, 0.028 mmol) and rifaldehyde (10 mg, 0.014 mmol). Yield: 4.4 mg, 35%, orange powder.

HRMS (ESI) *m/z*: $[M+H]^+$ calcd for $C_{47}H_{66}N_4O_{13}+H^+$: 895.4699; found: 895.4715.

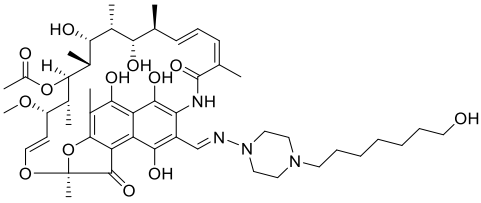

Compound 23. The compound was prepared according to General Procedure D, starting from alcohol **20** (6.1 mg, 0.028 mmol) and rifaldehyde (10 mg, 0.014 mmol). Yield: 4.4 mg, 34%, orange powder.

HRMS (ESI) *m/z*: $[M+H]^+$ calcd for $C_{49}H_{70}N_4O_{13}+H^+$: 923.5012; found: 923.5012.

General Procedure E (conjugation of piperazine-catechols with rifaldehyde). Rifaldehyde (10 mg, 0.014 mmol) and piperazine-catechol (0.028 mmol) were dissolved in dry THF (1 mL), and the resulting solution was left stirring for 2 h. After that, the reaction mixture was evaporated and then directly purified using the preparative HPLC method B. The fractions containing the pure product, as judged by HPLC, were combined and lyophilized to yield the desired conjugate.

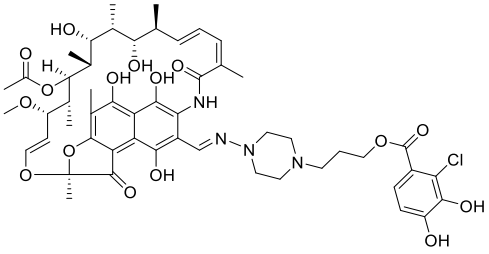

Conjugate 33. The compound was prepared according to General Procedure E, starting from piperazine-catechol **27** (9.2 mg, 0.028 mmol) and rifaldehyde (10 mg, 0.014 mmol). Yield: 7.6 mg, 52%, orange powder.

^{1}H NMR (600 MHz, DMSO-d_6) δ 12.38 (br s, 1H), 10.59 (br s, 1H), 10.17 (br s, 1H), 9.60 (br s, 1H), 9.43 (br s, 1H), 8.15 (s, 1H), 7.29 (d, J = 8.5 Hz, 1H), 6.98 – 6.88 (m, 1H), 6.81 (d, J = 8.5 Hz, 1H), 6.35 (d, J = 10.8 Hz, 1H), 6.26 (d, J = 12.7 Hz, 1H), 5.94 (dd, J = 15.8, 6.2 Hz, 1H), 5.05 (d, J = 10.9 Hz, 1H), 4.95 (dd, J = 12.8, 8.2 Hz, 1H), 4.27

(t, *J* = 6.1 Hz, 2H), 3.76 – 3.72 (m, 1H), 3.70 – 3.55 (m, 8H), 3.30 – 3.24 (m, 3H), 2.97 – 2.84 (m, 2H), 2.90 (s, 3H), 2.88 – 2.82 (m, 1H), 2.26 – 2.17 (m, 1H), 2.14 – 2.06 (m, 2H), 2.00 (s, 3H), 1.98 (s, 3H), 1.95 (s, 3H), 1.68 (s, 3H), 1.60 – 1.54 (m, 1H), 1.34 – 1.26 (m, 1H), 1.04 – 0.96 (m, 1H), 0.89 (d, *J* = 7.0 Hz, 3H), 0.82 (d, *J* = 6.9 Hz, 3H), 0.45 (d, *J* = 6.8 Hz, 3H), -0.33 (d, *J* = 6.7 Hz, 3H). **^{13}C{^{1}H} NMR** (151 MHz, DMSO-d_6) δ 172.5, 169.5, 167.2, 164.8, 150.2, 146.2, 143.0, 142.8, 137.3, 133.1, 131.0, 122.8, 120.4, 120.2, 118.3, 117.2, 117.1, 116.5, 115.2, 115.1, 113.7, 112.8, 108.8, 103.2, 102.8, 76.2, 76.0, 73.4, 71.5, 61.8, 55.7, 52.9, 49.9, 49.3, 48.6, 47.6, 47.4, 40.1, 38.4, 38.0, 34.4, 32.8, 23.1, 21.9, 20.7, 20.4, 17.6, 11.2, 8.8, 8.6, 7.5. **HRMS** (ESI) *m/z*: $[M+H]^+$ calcd for $C_{52}H_{65}ClN_4O_{16}+H^+$: 1037.4121; found: 1037.4161.

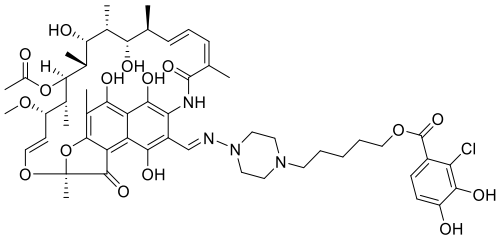

Conjugate 34. The compound was prepared according to General Procedure E, starting from piperazine-catechol **28** (10 mg, 0.028 mmol) and rifaldehyde (10 mg, 0.014 mmol). Yield: 6.8 mg, 46%, orange powder.

HRMS (ESI) *m/z*: $[M+H]^+$ calcd for $C_{54}H_{69}ClN_4O_{16}+H^+$: 1065.4470; found: 1065.4470.

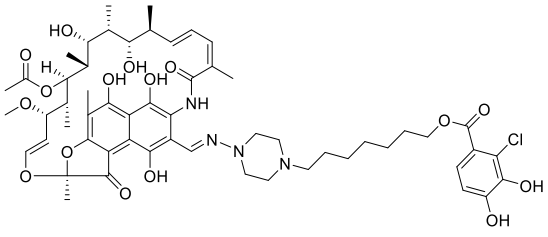

Conjugate 35. The compound was prepared according to General Procedure E, starting from piperazine-catechol **29** (10.8 mg, 0.028 mmol) and rifaldehyde (10 mg, 0.014 mmol). Yield: 5.8 mg, 38%, orange powder.

HRMS (ESI) *m/z*: $[M+H]^+$ calcd for $C_{56}H_{73}ClN_4O_{16}+H^+$: 1093.4783; found: 1093.4780.

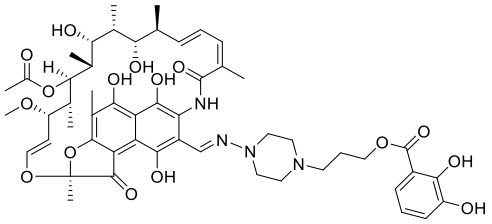

Conjugate 36. The compound was prepared according to General Procedure E, starting from piperazine-catechol **30** (8.2 mg, 0.028 mmol) and rifaldehyde (10 mg, 0.014 mmol). Yield: 5.1 mg, 36%, orange powder.

HRMS (ESI) *m/z*: $[M+H]^+$ calcd for $C_{52}H_{66}N_4O_{16}+H^+$: 1003.4547; found: 1003.4556.

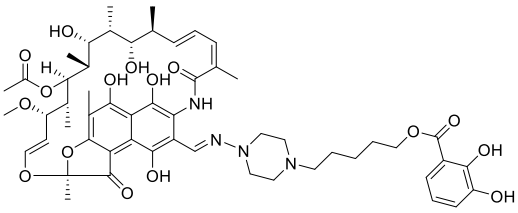

Conjugate 37. The compound was prepared according to General Procedure E, starting from piperazine-catechol **31** (9 mg, 0.028 mmol) and rifaldehyde (10 mg, 0.014 mmol). Yield: 4.7 mg, 33%, orange powder.

HRMS (ESI) *m/z*: $[M+H]^+$ calcd for $C_{54}H_{70}N_4O_{16}+H^+$: 1031.4860; found: 1031.4866.

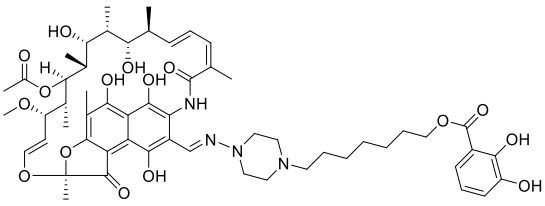

Conjugate 38. The compound was prepared according to General Procedure E, starting from piperazine-catechol **32** (9.8 mg, 0.028 mmol) and rifaldehyde (10 mg, 0.014 mmol). Yield: 4.4 mg, 30%, orange powder.

HRMS (ESI) *m/z*: $[M+H]^+$ calcd for $C_{56}H_{74}N_4O_{16}+H^+$: 1059.5173; found: 1059.5181.

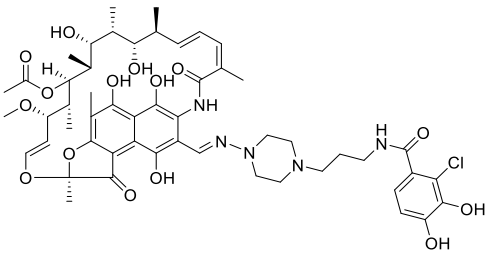

Conjugate 39. The compound was prepared according to General Procedure E, starting from piperazine-catechol **S12** (9.2 mg, 0.028 mmol) and rifaldehyde (10 mg, 0.014 mmol). Yield: 7.2 mg, 50%, orange powder.

HRMS (ESI) *m/z*: $[M+H]^+$ calcd for $C_{52}H_{66}ClN_5O_{15}+H^+$: 1036.4317; found: 1036.4310.

Synthesis of enterobactin

Enterobactin was synthesized following previously published methods with minor changes**.** Spectral data for all intermediates and enterobactin itself were in agreement with those reported in the literature.[48-51]

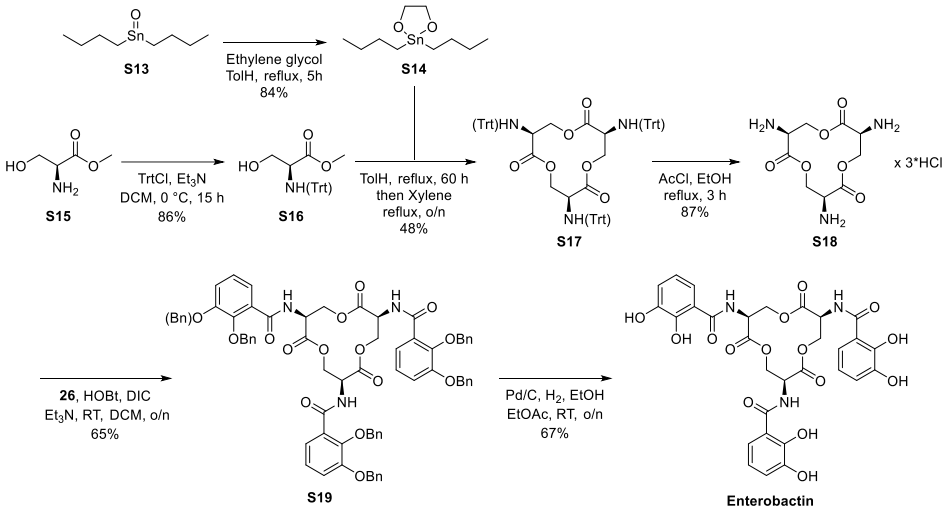

Scheme S4. Synthesis of enterobactin

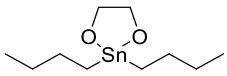

2,2-dibutyl-1,3,2-dioxastannolane (S14). Ethylene glycol (11.23 mL, 200 mmol) was added to a solution of dibutylstannanone (**S13**) (10 g, 40.2 mmol) in toluene (50 mL) at 25 °C. The reaction mixture was stirred at reflux for 5 hours. After gradually cooling from 110 °C to 20 °C, the precipitate was formed, filtered, washed with toluene, and dried at 40 °C under vacuum to give compound **S14** (9.9 g, 84% yield).

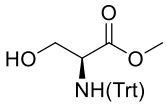

Methyl trityl-L-serinate (S16). To a suspension of L-Serine methyl ester hydrochloride (**S15**) (5 g, 32.2 mmol) in 50 mL of DCM at 0 °C, triethylamine (9 mL, 64.4 mmol) was added dropwise, followed by triphenylmethyl chloride (8.96 g, 32.2 mmol) in 20 mL of DCM. After stirring at RT for 15 h, the white precipitate formed was filtered off, and the filtrate evaporated in vacuo to yield a white solid, which was dissolved in EtOAc (200 mL) and washed with 10% citric acid (2 × 100 mL), saturated $NaHCO_3$ (100 mL), and water (2 × 100 mL). The separated organic layer was dried over Na_2SO_4, filtered, and concentrated in vacuo. The crude product was recrystallized from hexane to give compound **S16** (10.0 g, 86% yield) as a white solid.

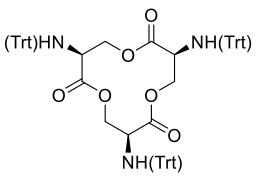

(3*S*,7*S*,11*S*)-3,7,11-tris(tritylamino)-1,5,9-trioxacyclododecane-2,6,10-trione (S17). Molecular sieves (20 g) and 2,2-dibutyl-1,3,2-dioxastannolane (**S14**) (0.41 g, 1.4 mmol) were added to a solution of methyl trityl-L-serinate (**S16**) in 150 mL of dry toluene, and the mixture was stirred at reflux for 60 h. Then, toluene was evaporated, and the residue was dissolved in xylene and stirred overnight at reflux. The resulting mixture was cooled to RT, filtered through a pad of Celite, and washed with 100 mL of toluene. Then, the filtrate was discarded, and the celite was washed with warm DCM (5 × 150 mL). The filtrate was evaporated, and the crude was diluted with MTBE (25 mL). The precipitate was formed, filtered, and washed with MTBE (10 mL) to obtain compound **S17** (2.2 g, 48% yield).

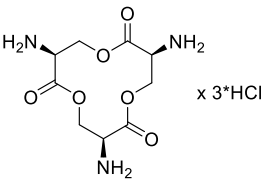

(3*S*,7*S*,11*S*)-3,7,11-triamino-1,5,9-trioxacyclododecane-2,6,10-trione trihydrochloride (S18). A dry solution of HCl was prepared by the reaction of acetyl chloride (0.35 mL, 4.86 mmol) with dry ethanol (30 mL). Then, a solution of the (3*S*,7*S*,11*S*)-3,7,11-tris(tritylamino)-1,5,9-trioxacyclododecane-2,6,10-trione (**S17**) (1.2 g, 1.21 mmol) in dry ethanol (10 mL) was added to the HCl solution and then refluxed for 30 minutes. The resulting mixture was concentrated to 15 mL under vacuum and cooled in an ice bath. The resulting solid was filtered, washed with cold, dry ethanol (5 mL), $CHCl_3$ (15 mL), and then Et_2O (2 × 15 mL), and dried to obtain compound **S18** (0.39 g, 87% yield) as a beige powder.

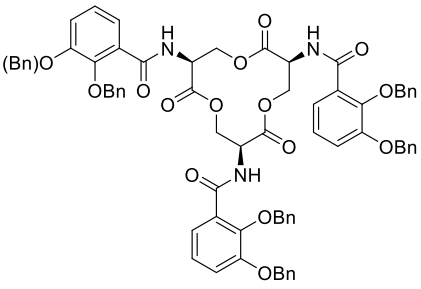

***N*,*N*',*N*"-((3*S*,7*S*,11*S*)-2,6,10-trioxo-1,5,9-trioxacyclododecane-3,7,11-triyl)-tris(2,3-bis(benzyloxy)-benzamide) (S19).** (3*S*,7*S*,11*S*)-3,7,11-triamino-1,5,9-trioxacyclododecane-2,6,10-trione tris hydrochloride (**S18**) (0.38 g, 1.03 mmol) was suspended in anhydrous DCM (12 mL) and treated with dry triethylamine (0.5 mL, 4.61 mmol) under Ar. The reaction mixture was stirred at RT for 10 min. Then, in a separate round-bottom flask, a mixture of 2,3-bis(benzyloxy)benzoic acid (**26**) (1.2 g, 3.59 mmol) and HOBt × H_2O (0.785 g, 5.13 mmol) was dissolved in anhydrous DCM (20 mL), followed by addition of DIC (0.65 g, 5.13 mmol) and stirred at RT for 20 min under Ar. Then, the solution of triseryl amine was added to the activated benzoic acid and stirred overnight at RT. The mixture was diluted with 20 mL of DCM and 50 mL of water. After extraction, the organic layer was separated, washed with 1 M HCl solution (25 mL), saturated $NaHCO_3$ solution (25 mL), water (25 mL), and brine (15 mL), then dried over Na_2SO_4 and concentrated in vacuo. The resulting residue was purified by silica gel column chromatography (SiO_2, EtOAc/PE) to afford compound **S19** (0.8 g, 65% yield) as a colorless liquid.

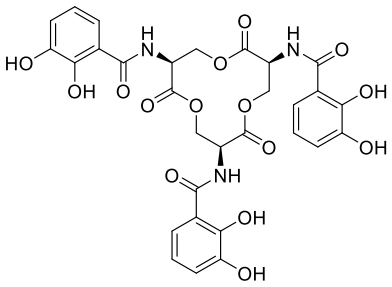

Enterobactin. *N*,*N*',*N*''-((3*S*,7*S*,11*S*)-2,6,10-trioxo-1,5,9-trioxacyclododecane-3,7,11-triyl)-tris(2,3-bis(benzyloxy)benzamide) (**S19**) (0.75 g, 0.62 mmol) was dissolved in a mixture of EtOH (5 mL) and EtOAc (5 mL) and hydrogenated in a round-bottom flask under balloon of hydrogen (1 bar) in presence of 10 % Pd/C (75 mg) overnight. The catalyst was filtered off, and the solvents were removed in vacuo to give the crude, which was purified by HPLC using method B to yield enterobactin (278 mg, 67% yield). **^{1}H NMR** (400 MHz, DMSO-d_6) δ 11.62 (s, 3H), 9.44 (br s, 3H), 9.11 (d, J = 6.9 Hz, 3H), 7.33 (dd, J = 8.2, 1.4 Hz, 3H), 6.96 (dd, J = 7.8, 1.4 Hz, 3H), 6.73 (t, J = 8.0 Hz, 3H), 4.89 (ddd, J = 9.2, 6.9, 4.7 Hz, 3H), 4.68 – 4.59 (m, 3H), 4.39 (dd, J = 10.9, 4.5 Hz, 3H). **^{13}C{^{1}H} NMR** (101 MHz, DMSO-d_6) δ 169.5, 169.0, 148.6, 146.2, 119.3, 118.5, 118.3, 115.29, 63.5, 51.3. **HRMS** (ESI) *m/z*: $[M+H]^+$ calcd for $C_{30}H_{27}N_3O_{15}+H^+$: 670.1515; found: 670.1520.

Supplementary information

Table S1. Activity of conjugate **33** and rifampicin in ID-CAMHB (iron-poor medium) against multiple wild-type *E. coli* BW 25113 strain and strains with different knockouts.

Strain	MIC (µg/mL)	
	33	Rifampicin
E. coli BW 25113	1	8
E. coli ΔtolC	1	4
E. coli ΔfepA	2	8
E. coli ΔfepB	1	4
E. coli ΔfepD	1	4
E. coli ΔfhuA	1	8
E. coli ΔfhuB	1	8
E. coli ΔfhuC	1	8
E. coli ΔfhuD	1	8
E. coli ΔfhuE	1	8
E. coli ΔfhuF	1	8
E. coli ΔentA	2	8
E. coli ΔentC	1	8

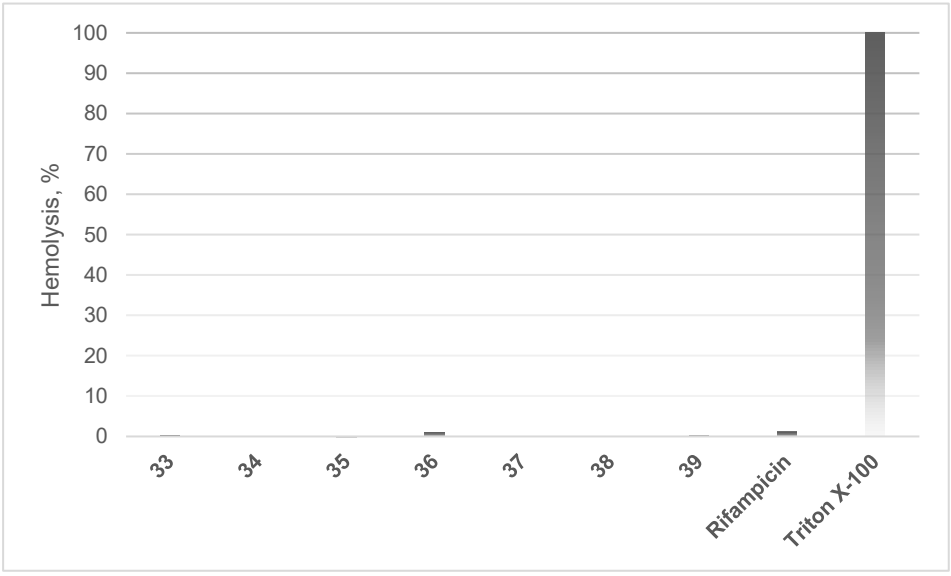

Figure S1. Hemolysis data (in %) for compounds 33-39 and rifampicin at a concentration of 64 µg/mL after 1 hour, compared to Triton X-100 (100%). The obtained values were used as the average of n = 3 technical replicates.

References

(1) Antimicrobial Resistance Collaborators. Global Burden of Bacterial Antimicrobial Resistance in 2019: A Systematic Analysis. *Lancet* **2022**, *399* (10325), 629−655.

(2) Prestinaci, F.; Pezzotti, P.; Pantosti, A. Antimicrobial Resistance: A Global Multifaceted Phenomenon. *Pathog Glob Health* **2015**, *109* (7), 309–318.

(3) GBD 2021 Antimicrobial Resistance Collaborators. Global Burden of Bacterial Antimicrobial Resistance 1990−2021: A Systematic Analysis with Forecasts to 2050. *Lancet* **2024**, *404* (10459), 1199–1226.

(4) Boucher, H. W.; Talbot, G. H.; Bradley, J. S.; Edwards, J. E.; Gilbert, D.; Rice, L. B.; Scheld, M.; Spellberg, B.; Bartlett, J. Bad Bugs, No Drugs: No ESKAPE! An Update from the Infectious Diseases Society of America. *Clin. Infect. Dis.* **2009**, *48* (1), 1–12.

(5) Gauba, A.; Rahman, K. M. Evaluation of Antibiotic Resistance Mechanisms in Gram-Negative Bacteria. *Antibiotics* **2023**, *12* (11), 1590.

(6) Breijyeh, Z.; Jubeh, B.; Karaman, R. Resistance of Gram-Negative Bacteria to Current Antibacterial Agents and Approaches to Resolve It. *Molecules* **2020**, *25* (6), 1340.

(7) Zgurskaya, H. I.; Rybenkov, V. V.; Krishnamoorthy, G.; Leus, I. V. Trans-Envelope Multidrug Efflux Pumps of Gram-Negative Bacteria and Their Synergism with the Outer Membrane Barrier. *Res. Microbiol.* **2018**, *169* (7–8), 351–356.

(8) Campbell, E. A.; Korzheva, N.; Mustaev, A.; Murakami, K.; Nair, S.; Goldfarb, A.; Darst, S. A. Structural Mechanism for Rifampicin Inhibition of Bacterial RNA Polymerase. *Cell* **2001**, *104* (6), 901–912.

(9) Floss, H. G.; Yu, T.-W. Rifamycin – Mode of Action, Resistance, and Biosynthesis. *Chem. Rev.* **2005**, *105* (2), 621–632.

(10) Grobbelaar, M.; Louw, G. E.; Sampson, S. L.; van Helden, P. D.; Donald, P. R.; Warren, R. M. Evolution of Rifampicin Treatment for Tuberculosis. *Infect. Genet. Evol.* **2019**, *74*, 103937.

(11) Thornsberry, C.; Hill, B. C.; Swenson, J. M.; Mcdougal, L. K. Vol. 5, Jul-Aug **1983** Supplement 3. The Use of Rifampin in the Treatment of Nontuberculous Infections. *Rev. Infect. Dis.*

(12) Drapeau, C. M. J.; Grilli, E.; Petrosillo, N. Rifampicin Combined Regimens for Gram-Negative Infections: Data from the Literature. *Int. J. Antimicrob. Agents* **2010**, *35* (1), 39–44.

(13) Jammal, J.; Zaknoon, F.; Kaneti, G.; Goldberg, K.; Mor, A. Sensitization of Gram-Negative Bacteria to Rifampin and OAK Combinations. *Sci. Rep.* **2015**, *5* (1), 9216.

(14) Wade, N.; Wesseling, C. M. J.; Innocenti, P.; Slingerland, C. J.; Koningstein, G. M.; Luirink, J.; Martin, N. I. Synthesis and Structure–Activity Studies of β-Barrel Assembly Machine Complex Inhibitor MRL-494. *ACS Infect. Dis.* **2022**, *8* (11), 2242–2252.

(15) Slingerland, C. J.; Kotsogianni, I.; Wesseling, C. M. J.; Martin, N. I. Polymyxin Stereochemistry and Its Role in Antibacterial Activity and Outer Membrane Disruption. *ACS Infect. Dis.* **2022**, *8* (12), 2396–2404.

(16) Rayner, B.; Verderosa, A. D.; Ferro, V.; Blaskovich, M. A. T. Siderophore Conjugates to Combat Antibiotic-Resistant Bacteria. *RSC Med. Chem.* **2023**, *14* (5), 800–822.

(17) Möllmann, U.; Heinisch, L.; Bauernfeind, A.; Köhler, T.; Ankel-Fuchs, D. Siderophores as Drug Delivery Agents: Application of the "Trojan Horse" Strategy. *BioMetals* **2009**, *22* (4), 615–624.

(18) Miller, M. J.; Malouin, F. Microbial Iron Chelators as Drug Delivery Agents: The Rational Design and Synthesis of Siderophore-Drug Conjugates. *Acc. Chem. Res.* **1993**, *26* (5), 241–249.

(19) Miethke, M.; Marahiel, M. A. Siderophore-Based Iron Acquisition and Pathogen Control. *Microbiol. Mol. Biol. Rev.* **2007**, *71* (3), 413–451.

(20) Wilson, B. R.; Bogdan, A. R.; Miyazawa, M.; Hashimoto, K.; Tsuji, Y. Siderophores in Iron Metabolism: From Mechanism to Therapy Potential. *Trends Mol. Med.* **2016**, *22* (12), 1077–1090.

(21) Schalk, I. J. Bacterial Siderophores: Diversity, Uptake Pathways and Applications. *Nat. Rev. Microbiol.* **2025**, *23* (1), 24–40.

(22) Raymond, K. N.; Dertz, E. A.; Kim, S. S. Enterobactin: An Archetype for Microbial Iron Transport. *Proc. Natl. Acad. Sci. U.S.A.* **2003**, *100* (7), 3584–3588.

(23) Abergel, R. J.; Warner, J. A.; Shuh, D. K.; Raymond, K. N. Enterobactin Protonation and Iron Release: Structural Characterization of the Salicylate Coordination Shift in Ferric Enterobactin[1]. *J. Am. Chem. Soc.* **2006**, *128* (27), 8920–8931.

(24) Page, M. G. P. Siderophore Conjugates. *Ann. N. Y. Acad. Sci.* **2013**, *1277* (1), 115–126.

(25) Page, M. G. P. The Role of Iron and Siderophores in Infection, and the Development of Siderophore Antibiotics. *Clin. Infect. Dis.* **2019**, *69* (Supplement_7), S529–S537.

(26) Peukert, C.; Vetter, A. C.; Fuchs, H. L. S.; Harmrolfs, K.; Karge, B.; Stadler, M.; Brönstrup, M. Siderophore Conjugation with Cleavable Linkers Boosts the Potency of RNA Polymerase Inhibitors against Multidrug-Resistant *E. Coli*. *Chem. Sci.* **2023**, *14* (20), 5490–5502.

(27) Trebosc, V.; Schellhorn, B.; Schill, J.; Lucchini, V.; Bühler, J.; Bourotte, M.; Butcher, J. J.; Gitzinger, M.; Lociuro, S.; Kemmer, C.; Dale, G. E. *In Vitro* Activity of Rifabutin against 293 Contemporary Carbapenem-Resistant *Acinetobacter Baumannii* Clinical Isolates and Characterization of Rifabutin Mode of Action and Resistance Mechanisms. *J. Antimicrob. Chemother.* **2020**, *75* (12), 3552–3562.

(28) Maingot, M.; Bourotte, M.; Vetter, A. C.; Schellhorn, B.; Antraygues, K.; Scherer, H.; Gitzinger, M.; Kemmer, C.; Dale, G. E.; Defert, O.; Lociuro, S.; Brönstrup, M.; Willand, N.; Trebosc, V. Structure-Activity Relationships of Actively FhuE Transported Rifabutin Derivatives with Potent Activity against Acinetobacter Baumannii. *Eur. J. Med. Chem.* **2023**, *252*, 115257.

(29) Ferguson, A. D.; Ködding, J.; Walker, G.; Bös, C.; Coulton, J. W.; Diederichs, K.; Braun, V.; Welte, W. Active Transport of an Antibiotic Rifamycin Derivative by the Outer-Membrane Protein FhuA. *Structure* **2001**, *9* (8), 707–716.

(30) Luna, B.; Trebosc, V.; Lee, B.; Bakowski, M.; Ulhaq, A.; Yan, J.; Lu, P.; Cheng, J.; Nielsen, T.; Lim, J.; Ketphan, W.; Eoh, H.; McNamara, C.; Skandalis, N.; She, R.; Kemmer, C.; Lociuro, S.; Dale, G. E.; Spellberg, B. A Nutrient-Limited Screen Unmasks Rifabutin Hyperactivity for Extensively Drug-Resistant Acinetobacter Baumannii. *Nat. Microbiol.* **2020**, *5* (9), 1134–1143.

(31) Karruli, A.; Massa, A.; Andini, R.; Marrazzo, T.; Ruocco, G.; Zampino, R.; Durante-Mangoni, E. Clinical Efficacy and Safety of Cefiderocol for Resistant Gram-Negative Infections: A Real-Life, Single-Centre Experience. *Int. J. Antimicrob. Agents* **2023**, *61* (2), 106723.

(32) El Ghali, A.; Kunz Coyne, A. J.; Lucas, K.; Tieman, M.; Xhemali, X.; Lau, S.; Iturralde, G.; Purdy, A.; Holger, D. J.; Garcia, E.; Veve, M. P.; Rybak, M. J. Cefiderocol: Early Clinical Experience for Multi-Drug Resistant Gram-Negative Infections. *Microbiol. Spectr.* **2024**, *12* (2), e0310823.

(33) Soriano, A.; Mensa, J. Mechanism of Action of Cefiderocol. *Spanish J. Chemother.* **2022**, *35* (Suppl2), 16–19.

(34) Pyta, K.; Przybylski, P.; Klich, K.; Stefańska, J. A New Model of Binding of Rifampicin and Its Amino Analogues as Zwitterions to Bacterial RNA Polymerase. *Org. Biomol. Chem.* **2012**, *10* (41), 8283.

(35) Pyta, K.; Janas, A.; Szukowska, M.; Pecyna, P.; Jaworska, M.; Gajecka, M.; Bartl, F.; Przybylski, P. Synthesis, Docking and Antibacterial Studies of More Potent Amine and Hydrazone Rifamycin Congeners than Rifampicin. *Eur. J. Med. Chem.* **2019**, *167*, 96–104.

(36) Zhao, R.; Zhu, J.; Jiang, X.; Bai, R. Click Chemistry-Aided Drug Discovery: A Retrospective and Prospective Outlook. *Eur. J. Med. Chem.* **2024**, *264*, 116037.

(37) Kolb, H. C.; Finn, M. G.; Sharpless, K. B. Click Chemistry: Diverse Chemical Function from a Few Good Reactions. *Angew. Chem. Int. Ed.* **2001**, *40* (11), 2004–2021.

(38) Devaraj, N. K.; Finn, M. G. Introduction: Click Chemistry. *Chem. Rev.* **2021**, *121* (12), 6697–6698.

(39) Idowu, T.; Arthur, G.; Zhanel, G. G.; Schweizer, F. Heterodimeric Rifampicin–Tobramycin Conjugates Break Intrinsic Resistance of Pseudomonas Aeruginosa to Doxycycline and Chloramphenicol in Vitro and in a Galleria Mellonella in Vivo Model. *Eur. J. Med. Chem.* **2019**, *174*, 16–32.

(40) Cochrane, S. A.; Li, X.; He, S.; Yu, M.; Wu, M.; Vederas, J. C. Synthesis of Tridecaptin–Antibiotic Conjugates with in Vivo Activity against Gram-Negative Bacteria. *J. Med. Chem.* **2015**, *58* (24), 9779–9785.

(41) Hackel, M. A.; Tsuji, M.; Yamano, Y.; Echols, R.; Karlowsky, J. A.; Sahm, D. F. Reproducibility of Broth Microdilution MICs for the Novel Siderophore Cephalosporin, Cefiderocol, Determined Using Iron-Depleted Cation-Adjusted Mueller-Hinton Broth. *Diagn. Microbiol. Infect. Dis.* **2019**, *94* (4), 321–325.

(42) Baba, T.; Ara, T.; Hasegawa, M.; Takai, Y.; Okumura, Y.; Baba, M.; Datsenko, K. A.; Tomita, M.; Wanner, B. L.; Mori, H. Construction of *Escherichia Coli* K-12 In-frame, Single-gene Knockout Mutants: The Keio Collection. *Mol. Syst. Biol.* **2006**, *2* (1).

(43) Yamamoto, K.; Yamamoto, N.; Ayukawa, S.; Yasutake, Y.; Ishiya, K.; Nakashima, N. Scaffold Size-Dependent Effect on the Enhanced Uptake of Antibiotics and Other Compounds by Escherichia Coli and Pseudomonas Aeruginosa. *Sci. Rep.* **2022**, *12* (1), 5609.

(44) Weinberg, S. E.; Villedieu, A.; Bagdasarian, N.; Karah, N.; Teare, L.; Elamin, W. F. Control and Management of Multidrug Resistant Acinetobacter Baumannii: A Review of the Evidence and Proposal of Novel Approaches. *Infect. Prev. Pract.* **2020**, *2* (3), 100077.

(45) Rafailidis, P.; Panagopoulos, P.; Koutserimpas, C.; Samonis, G. Current Therapeutic Approaches for Multidrug-Resistant and Extensively Drug-Resistant Acinetobacter Baumannii Infections. *Antibiotics* **2024**, *13* (3), 261.

(46) Vendrik, K. E. W.; de Haan, A.; Witteveen, S.; Hendrickx, A. P. A.; Landman, F.; Notermans, D. W.; Bijkerk, P.; Schoffelen, A. F.; de Greeff, S. C.; Wielders, C. C. H.; Goeman, J. J.; Kuijper, E. J.; Schouls, Leo. M.; Heemstra, K.; Vainio, S.; Ott, A.; de Jager, S.; Koene, F.; Hira, V.; van Burgel, N.; Muller, A.; Nagtegaal-Baerveldt, K.; van der Meer, C.; van den Biggelaar, R.; Pontesilli, O.; van Mens, S.; van den Bijllaardt, W.; Kolwijck, E.; Bosboom, R.; Frénay, I.; van 't Veen, A.; Troelstra, A.; Kampinga, G.; van Dijk, K. A Prospective Matched Case-Control Study on the Genomic Epidemiology of Colistin-Resistant Enterobacterales from Dutch Patients. *Commun. Med.* **2022**, *2* (1), 55.

(47) Khan, A. U.; Ali, A.; Danishuddin; Srivastava, G.; Sharma, A. Potential Inhibitors Designed against NDM-1 Type Metallo-β-Lactamases: An Attempt to Enhance Efficacies of Antibiotics against Multi-Drug-Resistant Bacteria. *Sci. Rep.* **2017**, *7* (1), 9207.

(48) Baramov, T.; Keijzer, K.; Irran, E.; Mösker, E.; Baik, M.; Süssmuth, R. Synthesis and Structural Characterization of Hexacoordinate Silicon, Germanium, and Titanium Complexes of the *E. Coli* Siderophore Enterobactin. *Chem. Eur. J.* **2013**, *19* (32), 10536–10542.

(49) Ramirez, R. J. A.; Karamanukyan, L.; Ortiz, S.; Gutierrez, C. G. A Much Improved Synthesis of the Siderophore Enterobactin. *Tetrahedron Lett.* **1997**, *38* (5), 749–752.

(50) Shanzer, A.; Libman, J. Total Synthesis of Enterobactin via an Organotin Template. *J. Chem. Soc. Chem. Commun.* **1983**, *15*, 846.

(51) Marinez, E. R.; Salmassian, E. K.; Lau, T. T.; Gutierrez, C. G. Enterobactin and Enantioenterobactin. *J. Org. Chem.* **1996**, *61* (10), 3548–3550.

(52) Pals, M. J.; Wijnberg, L.; Yildiz, Ç.; Velema, W. A. Catechol-Siderophore Mimics Convey Nucleic Acid Therapeutics into Bacteria. *Ang. Chem. Int. Ed.* **2024**, *63* (19).

(53) Tomaras, A. P.; Crandon, J. L.; McPherson, C. J.; Banevicius, M. A.; Finegan, S. M.; Irvine, R. L.; Brown, M. F.; O'Donnell, J. P.; Nicolau, D. P. Adaptation-Based Resistance to Siderophore-Conjugated Antibacterial Agents by Pseudomonas Aeruginosa. *Antimicrob. Agents Chemother.* **2013**, *57* (9), 4197–4207.

(54) Neumann, W.; Sassone-Corsi, M.; Raffatellu, M.; Nolan, E. M. Esterase-Catalyzed Siderophore Hydrolysis Activates an Enterobactin–Ciprofloxacin Conjugate and Confers Targeted Antibacterial Activity. *J. Am. Chem. Soc.* **2018**, *140* (15), 5193–5201.

(55) Schalk, I. J.; Mislin, G. L. A.; Brillet, K. Structure, Function and Binding Selectivity and Stereoselectivity of Siderophore–Iron Outer Membrane Transporters. *Curr. Top. Membr.* **2012**, 37–66.

(56) Stintzi, A.; Barnes, C.; Xu, J.; Raymond, K. N. Microbial Iron Transport via a Siderophore Shuttle: A Membrane Ion Transport Paradigm. *Proc. Natl. Acad. Sci. U.S.A.* **2000**, *97* (20), 10691–10696.

(57) Schatz, C.; Louguet, S.; Le Meins, J.; Lecommandoux, S. Polysaccharide- *Block* -polypeptide Copolymer Vesicles: Towards Synthetic Viral Capsids. *Ang. Chem. Int. Ed.* **2009**, *48* (14), 2572–2575.

(58) Vercillo, O. E.; Andrade, C. K. Z.; Wessjohann, L. A. Design and Synthesis of Cyclic RGD Pentapeptoids by Consecutive Ugi Reactions. *Org. Lett.* **2008**, *10* (2), 205–208.

(59) Hanna, J.; Allan, C.; Lawrence, C.; Meyer, O.; Wilson, N.; Hulme, A. Optimizing the Readout of Lanthanide-DOTA Complexes for the Detection of Ligand-Bound Copper(I). *Molecules* **2017**, *22* (5), 802.

(60) Chang, D.; Zhu, D.; Shi, L. [3 + 2] Cycloadditions of Azides with Arynes via Photolysis of Phthaloyl Peroxide Derivatives. *J. Org. Chem.* **2015**, *80* (11), 5928–5933.

(61) Gann, A. W.; Amoroso, J. W.; Einck, V. J.; Rice, W. P.; Chambers, J. J.; Schnarr, N. A. A Photoinduced, Benzyne Click Reaction. *Org. Lett.* **2014**, *16* (7), 2003–2005.

(62) Antoni, P.; Hed, Y.; Nordberg, A.; Nyström, D.; von Holst, H.; Hult, A.; Malkoch, M. Bifunctional Dendrimers: From Robust Synthesis and Accelerated One-Pot Postfunctionalization Strategy to Potential Applications. *Ang. Chem. Int. Ed.* **2009**, *48* (12), 2126–2130.

(63) Rossetti, A.; Sacchetti, A.; Meneghetti, F.; Colombo Dugoni, G.; Mori, M.; Castellano, C. Synthesis and Characterization of New Triazole-Bispidinone Scaffolds and Their Metal Complexes for Catalytic Applications. *Molecules* **2023**, *28* (17), 6351.

(64) Macerata, E.; Mossini, E.; Scaravaggi, S.; Mariani, M.; Mele, A.; Panzeri, W.; Boubals, N.; Berthon, L.; Charbonnel, M.-C.; Sansone, F.; Arduini, A.; Casnati, A. Hydrophilic Clicked 2,6-Bis-Triazolyl-Pyridines Endowed

with High Actinide Selectivity and Radiochemical Stability: Toward a Closed Nuclear Fuel Cycle. *J. Am. Chem. Soc.* **2016**, *138* (23), 7232–7235.

(65) Post, E. A. J.; Fletcher, S. P. Controlling the Kinetics of Self-Reproducing Micelles by Catalyst Compartmentalization in a Biphasic System. *J. Org. Chem.* **2019**, *84* (5), 2741–2755.

(66) Gracias, V.; Frank, K. E.; Milligan, G. L.; Aubé, J. Ring Expansion by in Situ Tethering of Hydroxy Azides to Ketones: The Boyer Reaction. *Tetrahedron* **1997**, *53* (48), 16241–16252.

(67) Chen, Y.-F.; Wu, C.-H.; Chen, L.-H.; Lee, H.-W.; Lee, J.-C.; Yeh, T.-K.; Chang, J.-Y.; Chou, M.-C.; Wu, H.-L.; Lai, Y.-P.; Song, J.-S.; Yeh, K.-C.; Chen, C.-T.; Lee, C.-J.; Shia, K.-S.; Shen, M.-R. Discovery of Potential Neuroprotective Agents against Paclitaxel-Induced Peripheral Neuropathy. *J. Med. Chem.* **2022**, *65* (6), 4767–4782.

(68) Zhang, J.; Jiang, J.; Li, Y.; Wan, X. Iodide-Catalyzed Synthesis of *N* -Nitrosamines via C–N Cleavage of Nitromethane. *J. Org. Chem.* **2013**, *78* (22), 11366–11372.